



**QUEEN'S  
UNIVERSITY  
BELFAST**

## Secure UAV-Enabled Communication Using Han-Kobayashi Signaling

Sheng, Z., Tuan, H. D., Nasir, A. A., Duong, T. Q., & Poor, H. V. (2020). Secure UAV-Enabled Communication Using Han-Kobayashi Signaling. *IEEE Transactions on Wireless Communications*, 19(5), 2905 - 2919. <https://doi.org/10.1109/TWC.2020.2968317>

### Published in:

IEEE Transactions on Wireless Communications

### Document Version:

Peer reviewed version

### Queen's University Belfast - Research Portal:

[Link to publication record in Queen's University Belfast Research Portal](#)

### Publisher rights

© 2020 The Authors.

This work is made available online in accordance with the publisher's policies. Please refer to any applicable terms of use of the publisher.

### General rights

Copyright for the publications made accessible via the Queen's University Belfast Research Portal is retained by the author(s) and / or other copyright owners and it is a condition of accessing these publications that users recognise and abide by the legal requirements associated with these rights.

### Take down policy

The Research Portal is Queen's institutional repository that provides access to Queen's research output. Every effort has been made to ensure that content in the Research Portal does not infringe any person's rights, or applicable UK laws. If you discover content in the Research Portal that you believe breaches copyright or violates any law, please contact [openaccess@qub.ac.uk](mailto:openaccess@qub.ac.uk).

### Open Access

This research has been made openly available by Queen's academics and its Open Research team. We would love to hear how access to this research benefits you. – Share your feedback with us: <http://go.qub.ac.uk/oa-feedback>

# Secure UAV-Enabled Communication Using Han-Kobayashi Signaling

Zhichao Sheng, Hoang D. Tuan, A. A. Nasir, Trung Q. Duong, and H. Vincent Poor

**Abstract**—This paper proposes Han-Kobayashi signaling (HK-S), under which each pair of users decodes a common message to improve their throughput, for UAV-enabled multi-user communication. Given that only a single transmit antenna is used and thus there is no null space of users' channels for inserting an artificial noise that would effectively help to jam an eavesdropper without interfering the users' desired signals, a new information and artificial noise transfer scheme to address physical layer security (PLS) for the considered networks is investigated. Under this scheme, the UAV sends the confidential information to its users within a fraction of the time slot and sends the artificial noise within the remaining fraction. Accordingly, the problem of jointly optimizing the time-fraction, bandwidth and power allocation to maximize the users' worst secrecy throughput is formulated. New inner approximations are proposed for developing path-following algorithms for its computation. Simulation shows that the proposed information and artificial noise transfer enables not only HKS but also orthogonal multi-access and nonorthogonal multi-access to provide PLS for UAV-enabled communication even when the eavesdropper is in the best channel condition. HKS outperforms the other two in terms of users' worst secrecy throughput.

**Index Terms**—Secure communication, secrecy throughput, unmanned aerial vehicle (UAV), Han-Kobayashi signaling, non-convex optimization,

## I. INTRODUCTION

Interference management is the key to achieving high throughput in multi-user communication, whose aim is to serve multiple users at the same time within a constrained bandwidth. In conventional orthogonal multi-access (OMA), each user decodes its own message by treating other messages as interference. Nonorthogonal multiple access (NOMA) [1], [2]

This work was supported in part by National Natural Science Foundation of China (NSFC) under Grant 61901254, in part by the Institute for Computational Science and Technology, Hochiminh City, Vietnam, in part by the Australian Research Councils' Discovery Projects under Project DP190102501, in part by the U.K. Royal Academy of Engineering Research Fellowship under Grant RF1415\14\22, in part by the U.S. National Science Foundation under Grants CCF-0939370 and CCF-1908308

Zhichao Sheng was with Queen's University Belfast, Belfast BT7 1NN, UK. He is now with Shanghai Institute for Advanced Communication and Data Science, the Key Laboratory of Specialty Fiber Optics and Optical Access Networks, Shanghai University, Shanghai 200444, China (email: zsheng@shu.edu.cn).

Hoang D. Tuan is with the school of Electrical and Data Engineering, University of Technology, Sydney, NSW 2007, Australia (email: tuan.hoang@uts.edu.au).

A. A. Nasir is with the Department of Electrical Engineering, King Fahd University of Petroleum and Minerals (KFUPM), Dhahran, Saudi Arabia (email: anasir@kfupm.edu.sa).

Trung Q. Duong is with Queen's University Belfast, Belfast BT7 1NN, UK (email: trung.q.duong@qub.ac.uk).

H. V. Poor is with the Department of Electrical Engineering, Princeton University, Princeton, NJ 08544, USA (email: poor@princeton.edu).

allows users with better channel conditions to decode messages for users with poorer channel conditions so the former can subtract these messages for the latter from their interference to decode their own messages with a better throughput outcome. By optimizing all their beamforming vectors, the throughput of all users can be substantially improved [3]. On the other hand, Han-Kobayashi signaling (HKS) [4] assigns a common message to each pair of users so that they can subtract this common message before decoding their own message to gain their throughput. Again, the throughput of all users can be substantially improved by beamforming optimization [5]–[7]. Recently, it has been shown in [8] that both OMA and NOMA are actually particular cases of HKS, and that unlike NOMA, the performance of HKS is not dependent on how the users' channel conditions are differentiated. All these aforementioned works exploit multiple transmit antennas, under which the wireless channels undergo rich scattering and transmit beamforming can enjoy the spatial diversity in delivering high throughput to the users. Rich scattering of wireless channels also plays a crucial role for ensuring physical layer security (PLS) [9]–[12], by aiding in achieving high secrecy throughput via secure beamforming [13]–[15].

Unmanned aerial vehicle (UAV)-enabled communication has attracted a lot of attention thanks to its high mobility and configuration flexibility [16]–[18]. The air-to-ground (A2G) channel between an UAV and a ground user is dominated by light-of-sight and thus is sufficiently strong for delivering high throughput. However, UAV-enabled communication preferably uses only a single transmit antenna as it is not beneficial to deploy multiple antennas due to A2G poor scattering. Thus, using single-antenna UAV, serving multiple users over orthogonal frequency bands is the only way to suppress the multi-user interference. It has been shown in [19] that the optimal bandwidth allocation to users' pairs to accommodate NOMA can bring much better users' throughput than the optimal bandwidth allocation to individual users to accommodate OMA, provided that the A2G channel gains between the UAV and each of the paired users are clearly distinct. A similar NOMA for UAV-enabled communication was also proposed [20].

Poor scattering also gives rise to insecure A2G channels, making them prone to being overheard by a ground eavesdropper (EV). In addition, the presence of a strong line-of-sight communication link strengthens the chance EV's attack. So, it is important to provide secure UAV-enabled communication. The closed-form analytical expressions for secrecy outage probability or average secrecy capacity were derived in [21] and [22]. PLS for a single A2G channel was considered

in [23]–[27]. The joint design of UAV trajectory/location and power optimization to maximize users’ secrecy throughput was addressed in [23]–[31]. Specifically, multiple potential eavesdroppers on the ground were considered with imperfect position information in [23], while in [25], an UAV was employed as a mobile jammer to combat against eavesdropping. In [26], both the downlink and uplink UAV communications were studied. In [27], the authors considered millimeter wave simultaneous wireless information and power transfer in UAV communications. Achieving secure communication over A2G channels is challenging because there is no null space of the user’s channel for inserting an artificial noise (AN) that would help to effectively jam the EV without interfering the users’ desired signals. To ensure secure communication, the authors in [28] optimized the UAV trajectory in such a way that would maximize the minimum secrecy throughput (among all users). In [24], [29]–[31], the authors used two UAVs in providing secure communication with one UAV delivering only information while the other sending only artificial noise to jam the EV(s). It is noteworthy that deploying a dynamic UAV or multiple stationary UAVs is too costly and thus not practical for secure communication. Beyond secure throughput, energy efficiency (EE) was considered for secure UAV-OFDMA systems in [32], where the joint design of transmit power, user scheduling, trajectory, and velocity for EE maximization was addressed. The main limitation of existing works [23]–[27] is that they do not consider multi-user communication. Specifically, different from the existing relevant works [23]–[32], we propose the use of HKS for UAV-enabled communication, which will be shown outperforming the performances of existing OMA and NOMA based UAV-enabled systems.

This paper investigates a multi-user communication system, where a single-antenna UAV aims to provide secure communication to multiple users in the presence of an EV. The location of the UAV, which can be optimized offline for a certain region, is fixed in order to save energy consumption that is a very critical issue in UAV-enabled communication. It has been shown in [33] that the energy consumption of a hovering UAV is the lowest when compared with that of a moving or circling UAV. The contributions and innovative aspects of this paper are as follows.

- This is the first work to propose HKS for UAV-enabled communication. Particularly, by jointly optimizing the bandwidth and power allocation, HKS is shown to achieve a sensible gain in terms of users’ throughput compared to OMA and NOMA [19].
- This is the first work in PLS that considers an EV which is placed in the best position to receive the strongest signal from the UAV. Without PLS, the EV thus can easily overhear this signal. On the other hand, there is no null space of users’ channels for inserting an artificial noise to jam the EV. To combat against the positioning advantage of the EV and to resolve the issue of jamming the EV, the paper proposes an innovative information and AN transfer, under which the UAV sends the confidential information to its users within a fraction

of a time slot and then sends the AN to jam the EV in the remaining fraction. The advantages of the time-fraction-wise transfer have been conveyed in [34]. In the context of PLS, the EV wiretaps the UAV signal on time-slot base, which is jammed by the inserted AN.

- Under the proposed information and AN transfer, the paper addresses the problem of jointly optimizing the time-fraction, power, and bandwidth allocation to maximize the users’ minimum secrecy throughput, which is seen as an extremely difficult nonconvex optimization problem with its decision variables entangled. Nevertheless, the paper proposes new inner approximation techniques for developing efficient path-following algorithms for its computations. The numerical examples demonstrate the advantages the proposed secure transmission, under which HKS also outperforms OMA and NOMA. Importantly, all of them offer a secure communication at low cost, which is not affected by the EV’s positioning.

*Notation.*  $[x]^+ \triangleq \max\{x, 0\}$  for a scalar  $x$ .  $n \sim \mathcal{CN}(\bar{n}, \sigma^2)$  indicates that  $n$  is circularly-symmetric complex Gaussian random variable with means  $\bar{n}$  and variance  $\sigma^2$ . The notation  $\sum_{j \neq i}^M$  refers to the summation taken over the index set  $\{1, \dots, M\} \setminus \{i\}$ . Optimization variables are in boldface.

The rest of the paper is organized as follows. Section II is devoted to secure HKS to protect an UAV-enabled communication from the EV’s overhearing over the whole bandwidth. Secure HKS to protect the EV’s overhearing in the allocated bandwidths is developed in Section III. The simulation is provided in Section IV to demonstrate the effectiveness of the proposed solutions and algorithms in the previous section. Conclusions are given in Section V. Some fundamental deterministic inequalities that are used in Sections II-III are given in the appendix.

## II. SECURE HKS FOR UAV-ENABLED COMMUNICATION

Consider a single-antenna UAV to serve  $K$  ground users (UEs) in a certain out-door location such as stadium, traffic jam, concert, etc., as depicted in Fig. 1. Obviously, these  $K$  UEs can be categorized into two groups of  $K/2$  UEs nearer (nearer UEs) to the UAV (in terms of Euclidean distance) and  $K/2$  UEs farther (farther UEs) to the UAV. Without loss of generality, we index the nearer UEs by  $k \in \{1, \dots, K/2\}$ , and the farther UEs by  $k \in \{K/2 + 1, \dots, K\}$ . Table I provides the nomenclature.

The channel between the UAV and UE  $k \in \{1, 2, \dots, K\}$ , denoted by  $g_k$  is given by

$$g_k = \frac{\sqrt{\gamma_o} \tilde{g}_k}{\theta(\|z_k - z_u\|^2 + h^2)^{\alpha/4}}, \quad (1)$$

where  $\gamma_o$  is the channel power gain at a reference distance of 1 m,  $z_k = (x_k, y_k)$  and  $z_u = (x_u, y_u)$  respectively are the coordinates of UE  $k$  and UAV on the horizontal ground plane,  $h$  is the UAV altitude,  $\theta$  is the UAV transmit-antenna beamwidth such that the UAV’s coverage radius  $R \leq h \tan \theta$ ,  $\alpha$  is the path loss exponent, and  $\tilde{g}_k \sim \mathcal{CN}(\mu, 2\sigma^2)$  represents the Rician distributed small-scale fading channel co-efficient with Rician factor  $K_R = |\mu|^2/2\sigma^2$  and normalized power  $\mathbb{E}(|\tilde{g}_k|^2) = 1$  [35].

TABLE I  
NOMENCLATURE.

| Notation                     | Description  |
|------------------------------|--|
| $K$                          | number of ground users   |
| $g_k$                        | channel between the UAV and UE $k$   |
| $g_E$                        | wiretap channel  |
| $\mathcal{B}$                | total bandwidth  |
| $\tau_k$                     | the portion of allocated bandwidth shared by UEs $k$ and $j(k)$              |
| $s_k / s_{j(k)}$             | private information for UE $k / j(k)$  |
| $s_{k,j(k)}$                 | common message for both UEs $k$ and $j(k)$                                   |
| $p_k / p_{j(k)}$             | power allocated to $s_k / s_{j(k)}$  |
| $p_{k,j(k)}$                 | power allocated to $s_{k,j(k)}$  |
| $r_k / r_{j(k)}$             | UE $k$ 's / $j(k)$ 's throughput by decoding $s_k / s_{j(k)}$                |
| $\rho_k / \rho_{j(k)}$       | secrecy throughput for UE $k / j(k)$   |
| $\rho_{k,c} / \rho_{j(k),c}$ | UE $k$ 's / $j(k)$ 's portion of secrecy throughput by decoding $s_{k,j(k)}$ |

Over the total bandwidth  $\mathcal{B}$ , UE  $k \in \{1, \dots, K/2\}$  is paired with UE  $j(k) = k + K/2$  in sharing the allocated bandwidth portion

$$b_k = \tau_k \mathcal{B}, \quad (2)$$

with  $0 < \tau_k < 1$ , for their service by the UAV.

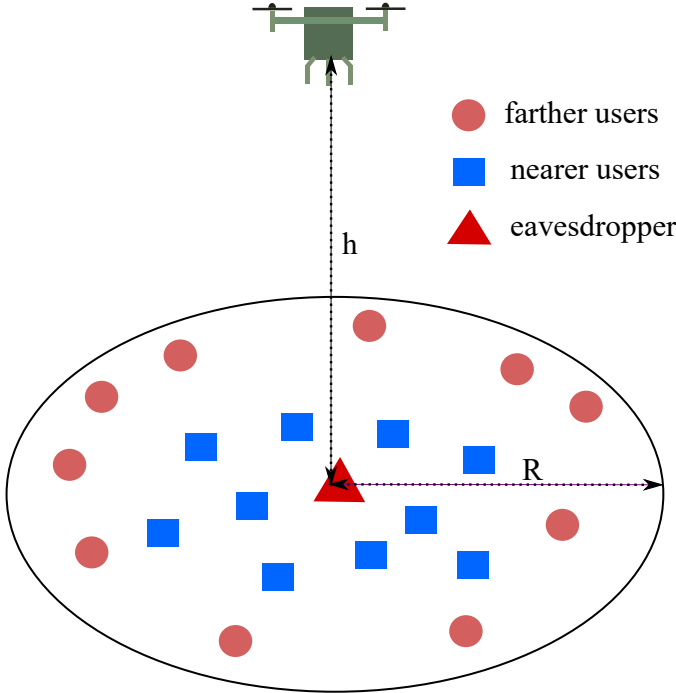


Fig. 1. A system model showing UAV-BS and the ground users.

Under HKS [4], the information intended for UEs  $k$  and  $j(k)$  is split as

$$s_k + s_{j(k)} + s_{k,j(k)}, \quad (3)$$

where  $s_k$  and  $s_{j(k)}$  contain private information for UEs  $k$  and  $j(k)$  while  $s_{k,j(k)}$  contains information for both UEs  $k$  and  $j(k)$ , which is called their common message. Accordingly, the equation for the received signals at UEs  $k$  and  $j(k)$  over the

shared bandwidth  $\mathcal{B}\tau_k$  is

$$\begin{aligned} \begin{bmatrix} y_k \\ y_{j(k)} \end{bmatrix} &= \begin{bmatrix} g_k \\ g_{j(k)} \end{bmatrix} (\sqrt{p_k} s_k + \sqrt{p_{j(k)}} s_{j(k)} + \sqrt{p_{k,j(k)}} s_{k,j(k)}) \\ &+ \begin{bmatrix} n_k \\ n_{j(k)} \end{bmatrix}, \end{aligned} \quad (4)$$

where  $n_k \sim \mathcal{CN}(0, \sigma_B \tau_k)$  and  $n_{j(k)} \sim \mathcal{CN}(0, \sigma_B \tau_k)$  are the background noise at the receiver of UEs  $k$  and  $j(k)$ , while  $p_k$ ,  $p_{j(k)}$ , and  $p_{k,j(k)}$  are the power allocated to  $s_k$ ,  $s_{j(k)}$ , and  $s_{k,j(k)}$ , respectively. Also,  $\sigma_n^2$  is the noise power density so  $\sigma_B \triangleq \sigma_n^2 \mathcal{B}$  is the noise power over the bandwidth  $\mathcal{B}$  and  $\sigma_B \tau_k$  is the noise power over the bandwidth  $\mathcal{B}\tau_k$ .

Let  $\boldsymbol{\tau} \triangleq (\tau_1, \dots, \tau_{K/2})^T$  and  $\mathbf{p} \triangleq (p_k, p_{j(k)}, p_{k,j(k)})_{k=1, \dots, K/2}$ . Under HKS [5], [7], both UEs  $k$  and  $j(k)$  decode their common message  $s_{k,j(k)}$  first with the throughput

$$r_{k,j(k)}(\boldsymbol{\tau}, \mathbf{p}) \triangleq \min\{r_{1,k,j(k)}(\boldsymbol{\tau}, \mathbf{p}), r_{2,k,j(k)}(\boldsymbol{\tau}, \mathbf{p})\}, \quad (5)$$

where

$$\begin{aligned} r_{i,k,j(k)}(\boldsymbol{\tau}, \mathbf{p}) &= \tau_k \ln \left( 1 + \frac{p_{k,j(k)}}{\nu_{i,k,j(k)}(\boldsymbol{\tau}, \mathbf{p})} \right), \quad i = 1, 2, \\ \nu_{1,k,j(k)}(\boldsymbol{\tau}, \mathbf{p}) &= \frac{\sigma_B}{|g_k|^2} \tau_k + p_k + p_{j(k)}, \\ \nu_{2,k,j(k)}(\boldsymbol{\tau}, \mathbf{p}) &= \frac{\sigma_B}{|g_{j(k)}|^2} \tau_k + p_k + p_{j(k)}. \end{aligned}$$

UEs  $k$  and  $j(k)$  then subtract  $s_{k,j(k)}$  from their received signal to decode  $s_k$  and  $s_{j(k)}$  with the throughput

$$\begin{aligned} r_k(\boldsymbol{\tau}, \mathbf{p}) &= \tau_k \ln \left( 1 + \frac{p_k}{\nu_k(\boldsymbol{\tau}, \mathbf{p})} \right), \\ \nu_k(\boldsymbol{\tau}, \mathbf{p}) &= \frac{\sigma_B}{|g_k|^2} \tau_k + p_{j(k)}, \end{aligned} \quad (6)$$

and

$$\begin{aligned} r_{j(k)}(\boldsymbol{\tau}, \mathbf{p}) &= \tau_k \ln \left( 1 + \frac{p_{j(k)}}{\nu_{j(k)}(\boldsymbol{\tau}, \mathbf{p})} \right), \\ \nu_{j(k)}(\boldsymbol{\tau}, \mathbf{p}) &= \frac{\sigma_B}{|g_{j(k)}|^2} \tau_k + p_k. \end{aligned} \quad (7)$$

We introduce the most challenging scenario for PLS when the UAV-enabled communication is overheard by an EV, which is located at the best position to wiretap the UAV signal as

shown by Fig. 1. Moreover, the wiretap channel  $g_E$  is assumed strongest as

$$g_E = \frac{\sqrt{\gamma_o}}{\theta h^{\alpha/2}}. \quad (8)$$

In this scenario, the EV does not know that the UEs are served in individual bandwidths, so it overhears  $s_{k,j(k)}$ ,  $s_k$  and  $s_{j(k)}$  over the whole bandwidth with the wiretapped throughput<sup>1</sup>

$$\rho_{k,j(k)}^E(\mathbf{p}) = \ln \left( 1 + \frac{p_{k,j(k)}}{\tilde{\lambda}_{k,j(k)}(\mathbf{p})} \right), \quad (9)$$

and

$$\rho_k^E(\mathbf{p}) = \ln \left( 1 + \frac{p_k}{\tilde{\lambda}_k(\mathbf{p})} \right), \quad (10)$$

and

$$\rho_{j(k)}^E(\mathbf{p}) = \ln \left( 1 + \frac{p_{j(k)}}{\tilde{\lambda}_{j(k)}(\mathbf{p})} \right), \quad (11)$$

where

$$\tilde{\lambda}_{k,j(k)}(\mathbf{p}) \triangleq \sum_{\ell \neq k}^{K/2} (p_\ell + p_{j(\ell)} + p_{\ell,j(\ell)}) + p_k + p_{j(k)} + \frac{\sigma_E}{|g_E|^2},$$

and

$$\tilde{\lambda}_k(\mathbf{p}) \triangleq \sum_{\ell \neq k}^{K/2} (p_\ell + p_{j(\ell)} + p_{\ell,j(\ell)}) + p_{k,j(k)} + p_{j(k)} + \frac{\sigma_E}{|g_E|^2},$$

and

$$\tilde{\lambda}_{j(k)}(\mathbf{p}) \triangleq \sum_{\ell \neq k}^{K/2} (p_\ell + p_{j(\ell)} + p_{\ell,j(\ell)}) + p_{k,j(k)} + p_k + \frac{\sigma_E}{|g_E|^2},$$

which are affine functions. Also  $\sigma_E \triangleq \sigma_e^2 \mathcal{B}$  for  $\sigma_e^2$  being the noise power density is the background noise power at the EV.

The secrecy throughput for UE  $k$  is

$$\rho_k(\boldsymbol{\tau}, \mathbf{p}) \triangleq [r_k(\boldsymbol{\tau}, \mathbf{p}) - \rho_k^E(\mathbf{p})]^+ + \boldsymbol{\rho}_{k,c}, \quad (12)$$

and the secrecy throughput for UE  $j(k)$  is

$$\rho_{j(k)}(\boldsymbol{\tau}, \mathbf{p}) \triangleq [r_{j(k)}(\boldsymbol{\tau}, \mathbf{p}) - \rho_{j(k)}^E(\mathbf{p})]^+ + \boldsymbol{\rho}_{j(k),c}, \quad (13)$$

where  $\boldsymbol{\rho}_{k,c}$  and  $\boldsymbol{\rho}_{j(k),c}$  satisfy

$$\boldsymbol{\rho}_{k,c} + \boldsymbol{\rho}_{j(k),c} \leq [r_{k,j(k)}(\boldsymbol{\tau}, \mathbf{p}) - \rho_{k,j(k)}^E(\mathbf{p})]^+, \quad (14)$$

because  $[r_{k,j(k)}(\boldsymbol{\tau}, \mathbf{p}) - \rho_{k,j(k)}^E(\mathbf{p})]^+$  is the secrecy throughput by decoding  $s_{k,j(k)}$  [4], [8].

Let  $\boldsymbol{\rho}_c \triangleq (\boldsymbol{\rho}_{k,c}, \boldsymbol{\rho}_{j(k),c})_{k=1, \dots, K/2}$ . The problem of max-min UEs' secrecy throughput optimization is formulated as

$$\max_{\substack{\boldsymbol{\tau} \in \mathbb{R}_+^{K/2}, \mathbf{p} \in \mathbb{R}_+^{3K/2}, \\ \boldsymbol{\rho}_c \in \mathbb{R}_+^K}} f(\boldsymbol{\tau}, \mathbf{p}, \boldsymbol{\rho}_c) \triangleq$$

$$\min_{k=1, \dots, K/2} \min \{ \rho_k(\boldsymbol{\tau}, \mathbf{p}), \rho_{j(k)}(\boldsymbol{\tau}, \mathbf{p}) \} \quad (15a)$$

$$\text{s.t.} \quad (14), \quad (15b)$$

$$\sum_{k=1}^{K/2} \tau_k \leq 1, \quad (15c)$$

$$\sum_{k=1}^{K/2} (p_k + p_{j(k)} + p_{k,j(k)}) \leq P, \quad (15d)$$

where the objective function in (15a) is the minimum of UEs' secrecy throughput, the constraints (15c) and (15d) respectively are the sum-bandwidth and sum transmit power constraints given a power budget  $P$ , and the constraint (14) splits the common secrecy throughput into individual secrecy throughput.

The objective function (15a) is nonconcave while the constraint (14) is nonconvex, making (15) a difficult nonconvex problem. To provide an efficient computation procedure we develop a technique of successive lower-bounding approximation for these functions, which is based on a lower-bounding concave function approximation for the UE throughput function and an upper-bounding convex function approximation for the wiretapped throughput function.

Let  $(\boldsymbol{\tau}^{(\kappa)}, \mathbf{p}^{(\kappa)})$  be the feasible point for (15) that is found from the  $(\kappa - 1)$ th iteration.

#### A. Successive UE's throughput function lower bounding approximation

Applying the inequality (69) in the appendix yields the following lower-bounding approximations:

$$\begin{aligned} r_k(\boldsymbol{\tau}, \mathbf{p}) &\geq r_k^{(\kappa)}(\boldsymbol{\tau}, \mathbf{p}) \\ &\triangleq a_k^{(\kappa)} - b_k^{(\kappa)} \left( \frac{\nu_k(\boldsymbol{\tau}, \mathbf{p})}{\nu_k(\boldsymbol{\tau}^{(\kappa)}, \mathbf{p}^{(\kappa)})} + \frac{p_k^{(\kappa)}}{p_k} \right) - \frac{c_k^{(\kappa)}}{\tau_k}, \end{aligned} \quad (16)$$

and

$$\begin{aligned} r_{j(k)}(\boldsymbol{\tau}, \mathbf{p}) &\geq r_{j(k)}^{(\kappa)}(\boldsymbol{\tau}, \mathbf{p}) \\ &\triangleq a_{j(k)}^{(\kappa)} - b_{j(k)}^{(\kappa)} \left( \frac{\nu_{j(k)}(\boldsymbol{\tau}, \mathbf{p})}{\nu_{j(k)}(\boldsymbol{\tau}^{(\kappa)}, \mathbf{p}^{(\kappa)})} + \frac{p_{j(k)}^{(\kappa)}}{p_{j(k)}} \right) \\ &\quad - \frac{c_{j(k)}^{(\kappa)}}{\tau_k}, \end{aligned} \quad (17)$$

and

$$\begin{aligned} r_{k,j(k)}(\boldsymbol{\tau}, \mathbf{p}) &\geq r_{k,j(k)}^{(\kappa)}(\boldsymbol{\tau}, \mathbf{p}) \\ &\triangleq \min \{ r_{1,k,j(k)}^{(\kappa)}(\boldsymbol{\tau}, \mathbf{p}), r_{2,k,j(k)}^{(\kappa)}(\boldsymbol{\tau}, \mathbf{p}) \}, \end{aligned} \quad (18)$$

<sup>1</sup>In some works such as [36], the denominator of (9) is incorrectly defined as  $\sum_{\ell \neq k}^{K/2} \tau_\ell (p_\ell + p_{j(\ell)} + p_{\ell,j(\ell)}) + \tau_k p_k + \tau_k p_{j(k)} + \frac{\sigma_E}{|g_E|^2}$ .

with

$$r_{i,k,j(k)}^{(\kappa)}(\boldsymbol{\tau}, \mathbf{p}) \triangleq a_{i,k,j(k)}^{(\kappa)} - b_{i,k,j(k)}^{(\kappa)} \left( \frac{\nu_{i,k,j(k)}(\boldsymbol{\tau}, \mathbf{p})}{\nu_{i,k,j(k)}(\tau^{(\kappa)}, p^{(\kappa)})} + \frac{p_{k,j(k)}^{(\kappa)}}{p_{k,j(k)}} \right) - \frac{c_{i,k,j(k)}^{(\kappa)}}{\tau_k}, \quad i = 1, 2,$$

where

$$\begin{aligned} 0 < a_k^{(\kappa)} &= 2r_k(\tau^{(\kappa)}, p^{(\kappa)}) + 2b_k^{(\kappa)}, \\ 0 < b_k^{(\kappa)} &= \tau_k^{(\kappa)} p_k^{(\kappa)} / (p_k^{(\kappa)} + \nu_k(\tau^{(\kappa)}, p^{(\kappa)})), \\ 0 < c_k^{(\kappa)} &= r_k(\tau^{(\kappa)}, p^{(\kappa)}) (\tau_k^{(\kappa)})^2, \end{aligned}$$

and

$$\begin{aligned} 0 < a_{j(k)}^{(\kappa)} &= 2r_{j(k)}(\tau^{(\kappa)}, p^{(\kappa)}) + 2b_{j(k)}^{(\kappa)}, \\ 0 < b_{j(k)}^{(\kappa)} &= \tau_{j(k)}^{(\kappa)} p_{j(k)}^{(\kappa)} / (p_{j(k)}^{(\kappa)} + \nu_{j(k)}(\tau^{(\kappa)}, p^{(\kappa)})), \\ 0 < c_{j(k)}^{(\kappa)} &= r_{j(k)}(\tau^{(\kappa)}, p^{(\kappa)}) (\tau_{j(k)}^{(\kappa)})^2, \end{aligned}$$

and

$$\begin{aligned} 0 < a_{i,k,j(k)}^{(\kappa)} &= 2r_{i,k,j(k)}(\tau^{(\kappa)}, p^{(\kappa)}) + 2b_{i,k,j(k)}^{(\kappa)}, \\ 0 < b_{i,k,j(k)}^{(\kappa)} &= \tau_{i,k,j(k)}^{(\kappa)} p_{i,k,j(k)}^{(\kappa)} / (p_{i,k,j(k)}^{(\kappa)} + \nu_{i,k,j(k)}(\tau^{(\kappa)}, p^{(\kappa)})), \\ 0 < c_{i,k,j(k)}^{(\kappa)} &= r_{i,k,j(k)}(\tau^{(\kappa)}, p^{(\kappa)}) (\tau_{i,k,j(k)}^{(\kappa)})^2, \quad i = 1, 2. \end{aligned}$$

Note that the functions  $r_k^{(\kappa)}$ ,  $r_{j(k)}^{(\kappa)}$  in (16) and (17), and  $r_{i,k,j(k)}^{(\kappa)}$  are concave. Then the function  $r_{k,j(k)}^{(\kappa)}$  in (18) is also concave as minimum of two concave functions [37].

### B. Successive EV's wiretapped throughput function upper bounding approximation

Applying the inequality (70) in the appendix yields

$$\begin{aligned} \rho_k^E(\mathbf{p}) &\leq -a_k^{E,(\kappa)} + \frac{0.5b_k^{E,(\kappa)}(p_k^2/p_k^{(\kappa)} + p_k^{(\kappa)})}{\tilde{\lambda}_k(\mathbf{p})} \\ &\triangleq \rho_k^{E,(\kappa)}(\mathbf{p}), \end{aligned} \quad (19)$$

where  $0 < a_k^{E,(\kappa)} = \bar{x}_k^{E,(\kappa)} b_k^{E,(\kappa)} - \ln(1 + \bar{x}_k^{E,(\kappa)})$ ,  $0 < b_k^{E,(\kappa)} = 1/(1 + \bar{x}_k^{E,(\kappa)})$ ,  $\bar{x}_k^{E,(\kappa)} = p_k^{(\kappa)} / \tilde{\lambda}_k(p^{(\kappa)})$ .

Analogously,

$$\begin{aligned} \rho_{j(k)}^E(\mathbf{p}) &\leq -a_{j(k)}^{E,(\kappa)} + \frac{0.5b_{j(k)}^{E,(\kappa)}(p_{j(k)}^2/p_{j(k)}^{(\kappa)} + p_{j(k)}^{(\kappa)})}{\tilde{\lambda}_{j(k)}(\mathbf{p})} \\ &\triangleq \rho_{j(k)}^{E,(\kappa)}(\mathbf{p}) \end{aligned} \quad (20)$$

and

$$\begin{aligned} \rho_{k,j(k)}^E(\mathbf{p}) &\leq -a_{k,j(k)}^{E,(\kappa)} + \frac{0.5b_{k,j(k)}^{E,(\kappa)}(p_{k,j(k)}^2/p_{k,j(k)}^{(\kappa)} + p_{k,j(k)}^{(\kappa)})}{\tilde{\lambda}_{k,j(k)}(\mathbf{p})} \\ &\triangleq \rho_{k,j(k)}^{E,(\kappa)}(\mathbf{p}) \end{aligned} \quad (21)$$

where  $0 < a_{j(k)}^{E,(\kappa)} = \bar{x}_{j(k)}^{E,(\kappa)} b_{j(k)}^{E,(\kappa)} - \ln(1 + \bar{x}_{j(k)}^{E,(\kappa)})$ ,  $0 < b_{j(k)}^{E,(\kappa)} = 1/(1 + \bar{x}_{j(k)}^{E,(\kappa)})$ ,  $\bar{x}_{j(k)}^{E,(\kappa)} = p_{j(k)}^{(\kappa)} / \tilde{\lambda}_{j(k)}(p^{(\kappa)})$ , and  $0 < a_{k,j(k)}^{E,(\kappa)} = \bar{x}_{k,j(k)}^{E,(\kappa)} b_{k,j(k)}^{E,(\kappa)} - \ln(1 + \bar{x}_{k,j(k)}^{E,(\kappa)})$ ,  $0 < b_{k,j(k)}^{E,(\kappa)} = 1/(1 + \bar{x}_{k,j(k)}^{E,(\kappa)})$ ,  $\bar{x}_{k,j(k)}^{E,(\kappa)} = p_{k,j(k)}^{(\kappa)} / \tilde{\lambda}_{k,j(k)}(p^{(\kappa)})$ .

All functions  $\rho_k^{E,(\kappa)}$ ,  $\rho_{j(k)}^{E,(\kappa)}$  and  $\rho_{k,j(k)}^{E,(\kappa)}$  are convex.

### C. Path-following algorithm

By using (16), (17), (18) and (19), (20), the secrecy throughput functions defined by (12), (13) are lower bounded by convex functions as follows:

$$\begin{aligned} \rho_\ell(\boldsymbol{\tau}, \mathbf{p}) &\geq \rho_\ell^{(\kappa)}(\boldsymbol{\tau}, \mathbf{p}) \\ &\triangleq r_\ell^{(\kappa)}(\boldsymbol{\tau}, \mathbf{p}) - \rho_\ell^{E,(\kappa)}(\mathbf{p}) + \boldsymbol{\rho}_{\ell,c}, \quad \ell \in \{k, j(k)\}, \end{aligned}$$

under the trust region

$$r_\ell^{(\kappa)}(\boldsymbol{\tau}, \mathbf{p}) - \rho_\ell^{E,(\kappa)}(\mathbf{p}) \geq 0, \quad \ell \in \{k, j(k)\}, \quad (22)$$

while the nonconvex constraint (14) is innerly approximated by the convex constraint

$$\boldsymbol{\rho}_{k,c} + \boldsymbol{\rho}_{j(k),c} \leq r_{i,k,j(k)}^{(\kappa)}(\boldsymbol{\tau}, \mathbf{p}) - \rho_{k,j(k)}^{E,(\kappa)}(\mathbf{p}), \quad i = 1, 2. \quad (23)$$

At the  $\kappa$ -th iteration the following convex optimization problem is solved to generate the next feasible point  $(\tau^{(\kappa+1)}, p^{(\kappa+1)}, \rho_c^{(\kappa+1)})$  for (15):

$$\begin{aligned} &\max_{\boldsymbol{\tau} \in \mathbb{R}_+^{K/2}, \mathbf{p} \in \mathbb{R}^{3K/2}, \boldsymbol{\rho}_c \in \mathbb{R}_+^K} f^{(\kappa)}(\boldsymbol{\tau}, \mathbf{p}, \boldsymbol{\rho}_c) = \\ &\min_{k=1, \dots, K/2} \min \left\{ \rho_k^{(\kappa)}(\boldsymbol{\tau}, \mathbf{p}), \rho_{j(k)}^{(\kappa)}(\boldsymbol{\tau}, \mathbf{p}) \right\} \end{aligned} \quad (24a)$$

$$\text{s.t. (15c), (15d), (22), (23).} \quad (24b)$$

The computational complexity of (24) is

$$\mathcal{O}(n^2 m^{2.5} + m^{3.5}), \quad (25)$$

where  $n = 3K$  is the number of decision variables, and  $m = 2K + 2$  is the number of constraints.

Note that  $(\tau^{(\kappa)}, p^{(\kappa)}, \rho_c^{(\kappa)})$  is feasible for (24), so

$$\begin{aligned} f^{(\kappa)}(\tau^{(\kappa+1)}, p^{(\kappa+1)}, \rho_c^{(\kappa+1)}) &> f^{(\kappa)}(\tau^{(\kappa)}, p^{(\kappa)}, \rho_c^{(\kappa)}) \\ &= f(\tau^{(\kappa)}, p^{(\kappa)}, \rho_c^{(\kappa)}). \end{aligned}$$

Therefore,

$$\begin{aligned} f(\tau^{(\kappa+1)}, p^{(\kappa+1)}, \rho_c^{(\kappa+1)}) &\geq f^{(\kappa)}(\tau^{(\kappa+1)}, p^{(\kappa+1)}, \rho_c^{(\kappa+1)}) \\ &> f(\tau^{(\kappa)}, p^{(\kappa)}, \rho_c^{(\kappa)}), \end{aligned}$$

i.e.  $(\tau^{(\kappa+1)}, p^{(\kappa+1)}, \rho_c^{(\kappa+1)})$  is a better feasible for (15) than  $(\tau^{(\kappa)}, p^{(\kappa)}, \rho_c^{(\kappa)})$ . As a result, the sequence  $\{(\tau^{(\kappa)}, p^{(\kappa)}, \rho_c^{(\kappa)})\}$  converges at least to a locally optimal solution of the nonconvex problem (15) [38]. Algorithm 1 summarizes the proposed computational procedure.

---

#### Algorithm 1 Secure HKS Algorithm

---

- 1: **Initialization:** Set  $\kappa = 0$ . Take any feasible point  $(\tau^{(0)}, p^{(0)}, \rho_c^{(0)})$  for the convex constraints (15c) and (15d).
  - 2: **Repeat until convergence:** Solve the convex optimization problem (24) to generate the next feasible point  $(\tau^{(\kappa+1)}, p^{(\kappa+1)}, \rho_c^{(\kappa+1)})$  for (15). Set  $\kappa := \kappa + 1$ .
  - 3: **Output**  $(\tau^{(\kappa)}, p^{(\kappa)}, \rho_c^{(\kappa)})$  as the optimal solution of (15).
-

#### D. Particular cases of secure HKS

Under HKS, the insecure (normal) throughput for UE  $k$  is  $r_k(\boldsymbol{\tau}, \mathbf{p}) + \boldsymbol{\rho}_{k,c}$  while the insecure throughput for UE  $j(k)$  is  $r_{j(k)}(\boldsymbol{\tau}, \mathbf{p}) + \boldsymbol{\rho}_{j(k),c}$ , where  $\boldsymbol{\rho}_{k,c}$  and  $\boldsymbol{\rho}_{j(k),c}$  satisfy

$$\boldsymbol{\rho}_{k,c} + \boldsymbol{\rho}_{j(k),c} \leq r_{k,j(k)}(\boldsymbol{\tau}, \mathbf{p}), \quad (26)$$

instead of (12), (13) and (14). The problem of max-min UEs' throughput optimization is simplified to

$$\begin{aligned} \max_{\boldsymbol{\tau} \in \mathbb{R}_+^{K/2}, \mathbf{p} \in \mathbb{R}_+^{3K/2}, \boldsymbol{\rho}_c \in \mathbb{R}_+^K} \quad & \min_{k=1, \dots, K/2} \min \{ r_k(\boldsymbol{\tau}, \mathbf{p}) + \boldsymbol{\rho}_{k,c}, \\ & r_{j(k)}(\boldsymbol{\tau}, \mathbf{p}) + \boldsymbol{\rho}_{j(k),c} \} \\ \text{s.t.} \quad & (15c), (15d), (26). \end{aligned} \quad (27)$$

Thus, Algorithm 2 for solving the problem (27) of max-min throughput optimization is a particular case of Algorithm 1. Therefore, the proof of convergence of Algorithm 2 can be similarly shown as that shown for Algorithm 1 below (25). The computational complexity of (27) can be expressed as (25) for  $n = 3K$  and  $m = K + 2$ .

---

#### Algorithm 2 Unsecure HKS Algorithm

---

- 1: **Initialization:** Set  $\kappa = 0$ . Take any feasible point  $(\tau^{(0)}, p^{(0)}, \rho_c^{(0)})$  for the convex constraints (15c) and (15d).
- 2: **Repeat until convergence:** For the functions  $r_k^{(\kappa)}(\boldsymbol{\tau}, \mathbf{p})$ ,  $r_{j(k)}^{(\kappa)}(\boldsymbol{\tau}, \mathbf{p})$ , and  $r_{k,j(k)}^{(\kappa)}(\boldsymbol{\tau}, \mathbf{p})$  respectively defined from (16), (17), and (18), solve the following convex optimization problem to generate the next feasible point  $(\tau^{(\kappa+1)}, p^{(\kappa+1)}, \rho_c^{(\kappa+1)})$  for (27):

$$\begin{aligned} \max_{\boldsymbol{\tau} \in \mathbb{R}_+^{K/2}, \mathbf{p} \in \mathbb{R}_+^{3K/2}, \boldsymbol{\rho}_c \in \mathbb{R}_+^K} \quad & \min_{k=1, \dots, K/2} \{ r_k^{(\kappa)}(\boldsymbol{\tau}, \mathbf{p}) \\ & + \boldsymbol{\rho}_{k,c}, r_{j(k)}^{(\kappa)}(\boldsymbol{\tau}, \mathbf{p}) + \boldsymbol{\rho}_{j(k),c} \} \end{aligned} \quad (28a)$$

$$\text{s.t.} \quad (15c), (15d), \quad (28b)$$

$$\boldsymbol{\rho}_{k,c} + \boldsymbol{\rho}_{j(k),c} \leq r_{k,j(k)}^{(\kappa)}(\boldsymbol{\tau}, \mathbf{p}). \quad (28c)$$

Set  $\kappa := \kappa + 1$ .

- 3: **Output**  $(\tau^{(\kappa)}, p^{(\kappa)}, \rho_c^{(\kappa)})$  as the optimal solution.
- 

It is obvious that user-pair-wise OMA is a particular case of HKS for  $s_{k,j(k)} = 0$  in (3), so  $\sqrt{p_{k,j(k)}} = 0$  in (4). However, such OMA is not better than the user-wise OMA, which allocates bandwidth to each user [19]. Furthermore, as pointed out in [8], NOMA is a particular case of HKS for  $s_{j(k)} = 0$  in (3) so  $\sqrt{p_{j(k)}} = 0$  in (4), and  $\boldsymbol{\rho}_{k,c} = 0$  in (26) so  $\boldsymbol{\rho}_{j(k),c} = r_{k,j(k)}(\boldsymbol{\tau}, \mathbf{p})$  because both UEs  $k$  and  $j(k)$  decode the message intended for UE  $j(k)$ . In other words, NOMA is a particular case of HKS where the common message is the entire message for UE  $j(k)$ , so the UEs' throughput can be optimized by Algorithm 2 by setting  $\boldsymbol{\rho}_{k,c} \equiv 0$  and  $r_{j(k)}(\boldsymbol{\tau}, \mathbf{p}) \equiv 0$  in (27). Similarly, secure NOMA is also seen as a particular case of secure HKS, thus its UEs' secrecy throughput can be optimized by Algorithm 1 by setting  $\boldsymbol{\rho}_{k,c} \equiv 0$  and  $r_{j(k)}(\boldsymbol{\tau}, \mathbf{p}) \equiv 0$  in (12), (13) and (14).

### III. INFORMATION AND ARTIFICIAL NOISE TRANSFER FOR SECURE HKS VERSUS OVERHEARING IN THE ALLOCATED BANDWIDTHS

One can see from (9)-(11) that PLS is improved with many more UEs served by the same UAV making the signal transmission over the whole bandwidth look sufficiently heterogeneous to the EV. In this section, we consider a even more favorable circumstance for the EV, under which it is able to detect the frequency center and the bandwidth portion allocated to UEs. The signal transmission over the allocated bandwidth for each pair of users is much less heterogeneous, making the wiretapped throughput easily high as the EV is with the best channel condition. Due to poor scattering of A2G channels as well as signal transmission by a single transmit antenna, there is no zero space of UEs' channels for inserting AN that would help to jam the EV without interfering the UEs' desired signals. Under this circumstance, the work [39] proposed to equip full-duplexes with the UEs, so while receiving the UAV signal the UEs also send an artificial noise to confuse the EV. Besides the technical challenges with providing such full-duplexes it was assumed in [39] that the EVs' receive can completely reject the signal sent by their transmitter that is never practical.

Now, we follow the approach firstly proposed in [13], which uses the power-signal for energy-transfer to confuse EV. The UAV uses the fraction  $0 < \mu = 1/t_1 < 1$  of the time-slot for transmitting information to the UEs and then uses the remaining fraction  $(1 - \mu) = 1/t_2$  to send an AN to confuse the EV.

For computational tractability, which will be clear in the later development, in this section, the power allocation to  $s_k$ ,  $s_{j(k)}$  and  $s_{k,j(k)}$  is respectively denoted by  $1/\sqrt{p_k}$ ,  $1/\sqrt{p_{j(k)}}$  and  $1/\sqrt{p_{k,j(k)}}$  while the bandwidth portion is denoted by  $1/\tau_k$ . Accordingly, the equation for the received signals at UEs  $k$  and  $j(k)$  over the shared bandwidth  $\mathcal{B}/\tau_k$  during the time fraction  $1/t_1$  is the following instead of (4):

$$\begin{bmatrix} y_k \\ y_{j(k)} \end{bmatrix} = \begin{bmatrix} g_k \\ g_{j(k)} \end{bmatrix} \left( \frac{s_k}{\sqrt{p_k}} + \frac{s_{j(k)}}{\sqrt{p_{j(k)}}} + \frac{s_{k,j(k)}}{\sqrt{p_{k,j(k)}}} \right) + \begin{bmatrix} n_k \\ n_{j(k)} \end{bmatrix}. \quad (29)$$

Let  $\boldsymbol{\tau} \triangleq (\tau_1, \dots, \tau_{K/2})^T$  and  $\mathbf{p} \triangleq \{ (p_k, p_{j(k)}, p_{k,j(k)}) : k = 1, \dots, K/2 \}$ . As the UEs are aware of the UAV transmission nature, they use (29) for decoding  $s_{k,j(k)}$ ,  $s_k$  and  $s_{j(k)}$  with the throughput  $\frac{1}{t_1} r_{k,j(k)}(\boldsymbol{\tau}, \mathbf{p})$ ,  $\frac{1}{t_1} r_k(\boldsymbol{\tau}, \mathbf{p})$ , and  $\frac{1}{t_1} r_{j(k)}(\boldsymbol{\tau}, \mathbf{p})$  with

$$r_{k,j(k)}(\boldsymbol{\tau}, \mathbf{p}) \triangleq \min \{ r_{1,k,j(k)}(\boldsymbol{\tau}, \mathbf{p}), r_{2,k,j(k)}(\boldsymbol{\tau}, \mathbf{p}) \}, \quad (30)$$

where

$$\begin{aligned} r_{i,k,j(k)}(\boldsymbol{\tau}, \mathbf{p}) &= \frac{1}{\tau_k} \ln \left( 1 + \frac{1}{p_{k,j(k)} \nu_{i,k,j(k)}(\boldsymbol{\tau}, \mathbf{p})} \right), \quad i = 1, 2, \\ \nu_{1,k,j(k)}(\boldsymbol{\tau}, \mathbf{p}) &= \frac{\sigma_B}{|g_k|^2 \tau_k} + \frac{1}{p_k} + \frac{1}{p_{j(k)}}, \\ \nu_{2,k,j(k)}(\boldsymbol{\tau}, \mathbf{p}) &= \frac{\sigma_B}{|g_{j(k)}|^2 \tau_k} + \frac{1}{p_k} + \frac{1}{p_{j(k)}}, \end{aligned}$$

and

$$\begin{aligned} r_k(\boldsymbol{\tau}, \mathbf{p}) &= \frac{1}{\tau_k} \ln \left( 1 + \frac{1}{p_k \nu_k(\boldsymbol{\tau}, \mathbf{p})} \right), \\ \nu_k(\boldsymbol{\tau}, \mathbf{p}) &= \frac{\sigma_B}{|g_k|^2 \tau_k} + \frac{1}{p_{j(k)}}, \end{aligned} \quad (31)$$

and

$$\begin{aligned} r_{j(k)}(\boldsymbol{\tau}, \mathbf{p}) &= \frac{1}{\tau_k} \ln \left( 1 + \frac{1}{p_{j(k)} \nu_{j(k)}(\boldsymbol{\tau}, \mathbf{p})} \right), \\ \nu_{j(k)}(\boldsymbol{\tau}, \mathbf{p}) &= \frac{\sigma_B}{|g_{j(k)}|^2 \tau_k} + \frac{1}{p_k}, \end{aligned} \quad (32)$$

instead of (5), (6), and (7).

The wiretapped signal by the EV over the bandwidth  $B/\tau_k$  during the time-fraction  $1/t_1 = \mu$  is

$$y_k^{E,1} = g_E \left( \frac{s_k}{\sqrt{p_k}} + \frac{s_{j(k)}}{\sqrt{p_{j(k)}}} + \frac{s_{k,j(k)}}{\sqrt{p_{k,j(k)}}} \right) + n_k^E, \quad (33)$$

and that during the time-fraction  $1/t_2 = 1 - \mu$  is

$$y_k^{E,2} = g_E \delta_k + n_k^E, \quad (34)$$

where  $\delta_k$  is the artificial noise of power  $1/p_k^E$  that the UAV sends to confuse EV and  $n_k^E$  is the EV's background noise of the power  $\sigma_E/\tau_k$ .

Since the EV overhears the time-slot-wise UAV signal, the signal  $y_k^{E,2}$  is considered as an AN. The noise power in decoding  $s_k$ ,  $s_{j(k)}$  and  $s_{k,j(k)}$  by the EV is

$$\frac{|g_E|^2}{t_2 p_k^E} + \frac{\sigma_E}{\tau_k}. \quad (35)$$

For  $\mathbf{p}^E \triangleq (p_1^E, \dots, p_{K/2}^E)$  and  $\mathbf{t} \triangleq (t_1, t_2)$ , the EV decodes  $s_{k,j(k)}$ ,  $s_k$  and  $s_{j(k)}$  with the throughput

$$r_{k,j(k)}^E(\boldsymbol{\tau}, \mathbf{p}, \mathbf{p}^E, \mathbf{t}) = \frac{1}{\tau_k} \ln \left( 1 + \frac{1/t_1 p_{k,j(k)}}{\nu_{k,j(k)}^E(\boldsymbol{\tau}, \mathbf{p}, \mathbf{p}^E, \mathbf{t})} \right), \quad (36)$$

and

$$r_k^E(\boldsymbol{\tau}, \mathbf{p}, \mathbf{p}^E, \mathbf{t}) = \frac{1}{\tau_k} \ln \left( 1 + \frac{1/t_1 p_k}{\nu_k^E(\boldsymbol{\tau}, \mathbf{p}, \mathbf{p}^E, \mathbf{t})} \right), \quad (37)$$

and

$$r_{j(k)}^E(\boldsymbol{\tau}, \mathbf{p}, \mathbf{p}^E, \mathbf{t}) = \frac{1}{\tau_k} \ln \left( 1 + \frac{1/t_1 p_{j(k)}}{\nu_{j(k)}^E(\boldsymbol{\tau}, \mathbf{p}, \mathbf{p}^E, \mathbf{t})} \right), \quad (38)$$

where

$$\nu_{k,j(k)}^E(\boldsymbol{\tau}, \mathbf{p}, \mathbf{p}^E, \mathbf{t}) \triangleq \frac{1}{t_1 p_k} + \frac{1}{t_1 p_{j(k)}} + \frac{1}{t_2 p_k^E} + \frac{\sigma_E}{|g_E|^2 \tau_k}, \quad (39)$$

and

$$\nu_k^E(\boldsymbol{\tau}, \mathbf{p}, \mathbf{p}^E, \mathbf{t}) \triangleq \frac{1}{t_1 p_{j(k)}} + \frac{1}{t_1 p_{k,j(k)}} + \frac{1}{t_2 p_k^E} + \frac{\sigma_E}{|g_E|^2 \tau_k}, \quad (40)$$

and

$$\nu_{j(k)}^E(\boldsymbol{\tau}, \mathbf{p}, \mathbf{p}^E, \mathbf{t}) \triangleq \frac{1}{t_1 p_k} + \frac{1}{t_1 p_{k,j(k)}} + \frac{1}{t_2 p_k^E} + \frac{\sigma_E}{|g_E|^2 \tau_k}. \quad (41)$$

Thus, the secrecy throughput for UE  $k$  is

$$r_k^S(\boldsymbol{\tau}, \mathbf{p}, \mathbf{p}^E, \mathbf{t}) \triangleq \left[ \frac{1}{t_1} r_k(\boldsymbol{\tau}, \mathbf{p}) - r_k^E(\boldsymbol{\tau}, \mathbf{p}, \mathbf{p}^E, \mathbf{t}) \right]^+ + r_{k,c}^S, \quad (42)$$

and the secrecy throughput for UE  $j(k)$  is

$$\begin{aligned} r_{j(k)}^S(\boldsymbol{\tau}, \mathbf{p}, \mathbf{p}^E, \mathbf{t}) &\triangleq \left[ \frac{1}{t_1} r_{j(k)}(\boldsymbol{\tau}, \mathbf{p}) - r_{j(k)}^E(\boldsymbol{\tau}, \mathbf{p}, \mathbf{p}^E, \mathbf{t}) \right]^+ \\ &\quad + r_{j(k),c}^S, \end{aligned} \quad (43)$$

where  $\mathbf{r}_{k,c}^S$  and  $\mathbf{r}_{j(k),c}^S$  satisfy

$$\mathbf{r}_{k,c}^S + \mathbf{r}_{j(k),c}^S \leq \left[ \frac{1}{t_1} r_{k,j(k)}(\boldsymbol{\tau}, \mathbf{p}) - r_{k,j(k)}^E(\boldsymbol{\tau}, \mathbf{p}, \mathbf{p}^E, \mathbf{t}) \right]^+, \quad (44)$$

because  $\left[ \frac{1}{t_1} r_{k,j(k)}(\boldsymbol{\tau}, \mathbf{p}) - r_{k,j(k)}^E(\boldsymbol{\tau}, \mathbf{p}, \mathbf{p}^E, \mathbf{t}) \right]^+$  is the secrecy throughput of  $s_{k,j(k)}$ .

Instead of (15d), the power constraint is

$$\sum_{k=1}^{K/2} \left[ \frac{1}{t_1 p_k} + \frac{1}{t_1 p_{j(k)}} + \frac{1}{t_1 p_{k,j(k)}} + \frac{1}{t_2 p_k^E} \right] \leq P, \quad (45)$$

which is imposed with the additional physical power constraints

$$\sum_{k=1}^{K/2} \left( \frac{1}{p_k} + \frac{1}{p_{j(k)}} + \frac{1}{p_{k,j(k)}} \right) \leq 3P, \quad (46)$$

and

$$\sum_{k=1}^{K/2} \frac{1}{p_k^E} \leq 3P. \quad (47)$$

The constraint for  $t_1 \geq 1$  and  $t_2 \geq 1$  is

$$\frac{1}{t_1} + \frac{1}{t_2} \leq 1. \quad (48)$$

Let  $\mathbf{r}_c^S \triangleq (\mathbf{r}_{k,c}^S, \mathbf{r}_{j(k),c}^S)_{k=1, \dots, K/2}$ . Instead of the problem (15) of UEs' max-min throughput optimization, we consider the following problem of UEs' max-min secrecy throughput optimization:

$$\begin{aligned} \max_{\substack{\boldsymbol{\tau} \in \mathbb{R}_+^{K/2}, \mathbf{p} \in \mathbb{R}_+^{3K/2}, \\ \mathbf{p}^E \in \mathbb{R}_+^{K/2}, \mathbf{t} \in \mathbb{R}_+^2, \\ \mathbf{r}_c^S \in \mathbb{R}_+^K}} f^S(\boldsymbol{\tau}, \mathbf{p}, \mathbf{p}^E, \mathbf{t}, \mathbf{r}_c^S) &\triangleq \end{aligned} \quad (49a)$$

$$\min_{k=1, \dots, K/2} \min \left\{ r_k^S(\boldsymbol{\tau}, \mathbf{p}, \mathbf{p}^E, \mathbf{t}), r_{j(k)}^S(\boldsymbol{\tau}, \mathbf{p}, \mathbf{p}^E, \mathbf{t}) \right\} \quad (49b)$$

$$\text{s.t.} \quad (44) - (48), \quad (49b)$$

$$\sum_{k=1}^{K/2} \frac{1}{\tau_k} \leq 1, \quad (49c)$$

where thanks to using  $1/t_i$  for expressing time-fractions, and  $1/p_k$  and  $1/p_k^E$  for expressing power allocations, all constraints (44)-(48) and (49c) are convex. Like (15), the computational difficulty of (49) is concentrated on its UEs' secrecy throughput functions that make the objective function (49a) nonconcave and the constraint (44) in (49b) nonconvex, which are much more complex than the UEs' secrecy throughput functions in the previous section.

Let  $(\tau^{(\kappa)}, p^{(\kappa)}, p^{E,(\kappa)}, t^{(\kappa)}, r_c^{S,(\kappa)})$  be the feasible point for (49) that is found from the  $(\kappa - 1)$ th iteration.



### A. Successive UEs' throughput function lower bounding approximation

Applying the inequality (66) in the appendix yields the following lower-bounding concave function approximations for UEs' throughput functions:

$$\begin{aligned} \frac{1}{t_1} r_k(\boldsymbol{\tau}, \mathbf{p}) &\geq a_k^{(\kappa)} + b_k^{(\kappa)} \left( 2 - \frac{\nu_k(\boldsymbol{\tau}, \mathbf{p})}{\nu_k(\tau^{(\kappa)}, p^{(\kappa)})} - \frac{p_k}{p_k^{(\kappa)}} \right) \\ &\quad - c_k^{(\kappa)} t_1 - d_k^{(\kappa)} \tau_k \\ &\triangleq f_k^{(\kappa)}(\boldsymbol{\tau}, \mathbf{p}, \mathbf{t}), \end{aligned} \quad (50)$$

and

$$\begin{aligned} \frac{1}{t_1} r_{j(k)}(\boldsymbol{\tau}, \mathbf{p}) &\geq a_{j(k)}^{(\kappa)} + b_{j(k)}^{(\kappa)} \left( 2 - \frac{\nu_{j(k)}(\boldsymbol{\tau}, \mathbf{p})}{\nu_{j(k)}(\tau^{(\kappa)}, p^{(\kappa)})} \right. \\ &\quad \left. - \frac{p_{j(k)}}{p_{j(k)}^{(\kappa)}} \right) - c_{j(k)}^{(\kappa)} t_1 - d_{j(k)}^{(\kappa)} \tau_k \\ &\triangleq f_{j(k)}^{(\kappa)}(\boldsymbol{\tau}, \mathbf{p}, \mathbf{t}), \end{aligned} \quad (51)$$

and

$$\begin{aligned} \frac{1}{t_1} r_{k,j(k)}(\boldsymbol{\tau}, \mathbf{p}) &= \min \left\{ \frac{1}{t_1} r_{1,k,j(k)}(\boldsymbol{\tau}, \mathbf{p}), \frac{1}{t_1} r_{2,k,j(k)}(\boldsymbol{\tau}, \mathbf{p}) \right\} \\ &\geq \min \{ f_{1,k,j(k)}^{(\kappa)}(\boldsymbol{\tau}, \mathbf{p}, \mathbf{t}), f_{2,k,j(k)}^{(\kappa)}(\boldsymbol{\tau}, \mathbf{p}, \mathbf{t}) \} \\ &\triangleq f_{k,j(k)}^{(\kappa)}(\boldsymbol{\tau}, \mathbf{p}, \mathbf{t}), \end{aligned} \quad (52)$$

with

$$\begin{aligned} f_{i,k,j(k)}^{(\kappa)}(\boldsymbol{\tau}, \mathbf{p}, \mathbf{t}) &= a_{i,k,j(k)}^{(\kappa)} + b_{i,k,j(k)}^{(\kappa)} \\ &\quad \times \left( 2 - \frac{\nu_{i,k,j(k)}(\boldsymbol{\tau}, \mathbf{p})}{\nu_{i,k,j(k)}(\tau^{(\kappa)}, p^{(\kappa)})} - \frac{p_{k,j(k)}}{p_{k,j(k)}^{(\kappa)}} \right) \\ &\quad - c_{i,k,j(k)}^{(\kappa)} t_1 - d_{i,k,j(k)}^{(\kappa)} \tau_k, \quad i = 1, 2, \end{aligned} \quad (53)$$

where

$$\begin{aligned} 0 < a_k^{(\kappa)} &= \frac{3}{t_1^{(\kappa)}} r_k(\tau^{(\kappa)}, p^{(\kappa)}), \\ 0 < b_k^{(\kappa)} &= \frac{1}{t_1^{(\kappa)} \tau_k^{(\kappa)} (1 + \nu_k(\tau^{(\kappa)}, p^{(\kappa)}) p_k^{(\kappa)})}, \\ 0 < c_k^{(\kappa)} &= \frac{1}{(t_1^{(\kappa)})^2} r_k(\tau^{(\kappa)}, p^{(\kappa)}), \\ 0 < d_k^{(\kappa)} &= \frac{1}{t_1^{(\kappa)} \tau_k^{(\kappa)}} r_k(\tau^{(\kappa)}, p^{(\kappa)}), \end{aligned}$$

and

$$\begin{aligned} 0 < a_{j(k)}^{(\kappa)} &= \frac{3}{t_1^{(\kappa)}} r_{j(k)}(\tau^{(\kappa)}, p^{(\kappa)}), \\ 0 < b_{j(k)}^{(\kappa)} &= \frac{1}{t_1^{(\kappa)} \tau_k^{(\kappa)} (1 + \nu_{j(k)}(\tau^{(\kappa)}, p^{(\kappa)}) p_{j(k)}^{(\kappa)})}, \\ 0 < c_{j(k)}^{(\kappa)} &= \frac{1}{(t_1^{(\kappa)})^2} r_{j(k)}(\tau^{(\kappa)}, p^{(\kappa)}), \\ 0 < d_{j(k)}^{(\kappa)} &= \frac{1}{t_1^{(\kappa)} \tau_k^{(\kappa)}} r_{j(k)}(\tau^{(\kappa)}, p^{(\kappa)}), \end{aligned}$$

and, for  $i = 1, 2$ ,

$$\begin{aligned} 0 < a_{i,k,j(k)}^{(\kappa)} &= \frac{3}{t_1^{(\kappa)}} r_{i,k,j(k)}(\tau^{(\kappa)}, p^{(\kappa)}), \\ 0 < b_{i,k,j(k)}^{(\kappa)} &= \frac{1}{t_1^{(\kappa)} \tau_k^{(\kappa)} (1 + \nu_{i,k,j(k)}(\tau^{(\kappa)}, p^{(\kappa)}) p_{k,j(k)}^{(\kappa)})}, \\ 0 < c_{i,k,j(k)}^{(\kappa)} &= \frac{1}{(t_1^{(\kappa)})^2} r_{i,k,j(k)}(\tau^{(\kappa)}, p^{(\kappa)}), \\ 0 < d_{i,k,j(k)}^{(\kappa)} &= \frac{1}{t_1^{(\kappa)} \tau_k^{(\kappa)}} r_{i,k,j(k)}(\tau^{(\kappa)}, p^{(\kappa)}). \end{aligned}$$

### B. Successive EV's wiretapped throughput function upper bounding approximation

In regard to EV's wiretapped throughput functions in (36), (37), and (38), applying the inequality (67) in the appendix yields their following approximations

$$\begin{aligned} r_k^E(\boldsymbol{\tau}, \mathbf{p}, \mathbf{p}^E, \mathbf{t}) &\leq -\frac{a_k^{E,(\kappa)}}{\tau_k} + \frac{b_k^{E,(\kappa)}}{t_1 p_k \tau_k \nu_k^E(\boldsymbol{\tau}, \mathbf{p}, \mathbf{p}^E, \mathbf{t})} \\ &\leq -a_k^{E,(\kappa)} \left( \frac{2}{\tau_k^{(\kappa)}} - \frac{\tau_k}{(\tau_k^{(\kappa)})^2} \right) + \frac{b_k^{E,(\kappa)}}{t_1 p_k \lambda_k(\mathbf{z})} \\ &\triangleq f_k^{E,(\kappa)}(\boldsymbol{\tau}, \mathbf{p}, \mathbf{p}^E, \mathbf{t}, \mathbf{z}), \end{aligned} \quad (54)$$

where

$$\begin{aligned} 0 < a_k^{E,(\kappa)} &= \bar{x}_k^{E,(\kappa)} b_k^{E,(\kappa)} - \ln \left( 1 + \bar{x}_k^{E,(\kappa)} \right), \\ 0 < b_k^{E,(\kappa)} &= 1 / (1 + \bar{x}_k^{E,(\kappa)}), \\ \bar{x}_k^{E,(\kappa)} &= 1 / t_1^{(\kappa)} p_k^{(\kappa)} \nu_k^E(\tau^{(\kappa)}, p^{(\kappa)}, p^E, t^{(\kappa)}), \end{aligned}$$

and  $\lambda_k(\mathbf{z}) \triangleq z_{j(k)} + z_{k,j(k)} + z_k^E + \sigma_E / |g_E|^2$ , which is an affine lower bounding approximation of the nonlinear function  $\tau_k \nu_k^E(\boldsymbol{\tau}, \mathbf{p}, \mathbf{p}^E, \mathbf{t})$ , provided that

$$z_{j(k)} \leq \tau_k / t_1 p_{j(k)} \Leftrightarrow \frac{1}{\tau_k} \leq \frac{1}{z_{j(k)} t_1 p_{j(k)}}, \quad (55a)$$

$$z_{k,j(k)} \leq \tau_k / t_1 p_{k,j(k)} \Leftrightarrow \frac{1}{\tau_k} \leq \frac{1}{z_{k,j(k)} t_1 p_{k,j(k)}}, \quad (55b)$$

$$z_k^E \leq \tau_k / t_2 p_k^E \Leftrightarrow \frac{1}{\tau_k} \leq \frac{1}{z_k^E t_2 p_k^E}. \quad (55c)$$

Applying the inequality (68) in the appendix for  $x = t_1$ ,  $y = p_{j(k)}$ ,  $z = z_{j(k)}$  and  $\bar{x} = t_1^{(\kappa)}$ ,  $\bar{y} = p_{j(k)}^{(\kappa)}$ ,  $\bar{z} = \tau_k^{(\kappa)} / t_1^{(\kappa)} p_{j(k)}^{(\kappa)}$  yields the following inner convex approximation for the nonconvex constraint (55a):

$$\frac{1}{\tau_k} \leq \frac{1}{\tau_k^{(\kappa)}} \left[ 4 - t_1^{(\kappa)} p_{j(k)}^{(\kappa)} \frac{z_{j(k)}}{\tau_k^{(\kappa)}} - \frac{t_1}{t_1^{(\kappa)}} - \frac{p_{j(k)}}{p_{j(k)}^{(\kappa)}} \right], \quad z_{j(k)} > 0. \quad (56)$$

Analogously, the nonconvex constraints (55b) and (55c) are innerly approximated by the following convex constraints:

$$\frac{1}{\tau_k} \leq \frac{1}{\tau_k^{(\kappa)}} \left[ 4 - t_1^{(\kappa)} p_{k,j(k)}^{(\kappa)} \frac{z_{k,j(k)}}{\tau_k^{(\kappa)}} - \frac{t_1}{t_1^{(\kappa)}} - \frac{p_{k,j(k)}}{p_{k,j(k)}^{(\kappa)}} \right], \quad z_{k,j(k)} > 0, \quad (57)$$

$$\frac{1}{\tau_k} \leq \frac{1}{\tau_k^{(\kappa)}} \left[ 4 - t_2^{(\kappa)} p_k^{E,(\kappa)} \frac{z_k^E}{\tau_k^{(\kappa)}} - \frac{t_2}{t_2^{(\kappa)}} - \frac{p_k^E}{p_k^{E,(\kappa)}} \right], z_k^E > 0. \quad (58)$$

By using a similar argument,

$$\begin{aligned} r_{j(k)}^E(\boldsymbol{\tau}, \mathbf{p}, \mathbf{p}^E, \mathbf{t}) &\leq f_{j(k)}^{E,(\kappa)}(\boldsymbol{\tau}, \mathbf{p}, \mathbf{p}^E, \mathbf{t}, \mathbf{z}) \\ &\triangleq -a_{j(k)}^{E,(\kappa)} \left( \frac{2}{\tau_k^{(\kappa)}} - \frac{\tau_k}{(\tau_k^{(\kappa)})^2} \right) \\ &\quad + \frac{b_{j(k)}^{E,(\kappa)}}{t_1 p_{j(k)} \lambda_{j(k)}(\mathbf{z})} \end{aligned} \quad (59)$$

over the trust region (57) and (58) and

$$\frac{1}{\tau_k} \leq \frac{1}{\tau_k^{(\kappa)}} \left[ 4 - t_1^{(\kappa)} p_k^{(\kappa)} \frac{z_k}{\tau_k^{(\kappa)}} - \frac{t_1}{t_1^{(\kappa)}} - \frac{p_k}{p_k^{(\kappa)}} \right], z_k > 0, \quad (60)$$

with

$$\begin{aligned} 0 < a_{j(k)}^{E,(\kappa)} &= \bar{x}_{j(k)}^{E,(\kappa)} b_{j(k)}^{E,(\kappa)} - \ln \left( 1 + \bar{x}_{j(k)}^{E,(\kappa)} \right), \\ 0 < b_{j(k)}^{E,(\kappa)} &= 1 / (1 + \bar{x}_{j(k)}^{E,(\kappa)}), \\ \bar{x}_{j(k)}^{E,(\kappa)} &= 1 / t_1^{(\kappa)} p_{j(k)}^{(\kappa)} \nu_{j(k)}^E(\tau^{(\kappa)}, p^{(\kappa)}, p^{E,(\kappa)}, t^{(\kappa)}), \end{aligned}$$

and  $\lambda_{j(k)}(\mathbf{z}) \triangleq z_k + z_{k,j(k)} + z_k^E + \sigma_E / |g_E|^2$ , which is an affine lower bounding approximation of the nonlinear function  $\tau_k \nu_{j(k)}^E(\boldsymbol{\tau}, \mathbf{p}, \mathbf{p}^E, \mathbf{t})$ .

Furthermore,

$$\begin{aligned} r_{k,j(k)}^E(\boldsymbol{\tau}, \mathbf{p}, \mathbf{p}^E, \mathbf{t}) &\leq f_{k,j(k)}^{E,(\kappa)}(\boldsymbol{\tau}, \mathbf{p}, \mathbf{p}^E, \mathbf{t}, \mathbf{z}) \\ &\triangleq -a_{k,j(k)}^{E,(\kappa)} \left( \frac{2}{\tau_k^{(\kappa)}} - \frac{\tau_k}{(\tau_k^{(\kappa)})^2} \right) \\ &\quad + \frac{b_{k,j(k)}^{E,(\kappa)}}{t_1 p_{k,j(k)} \lambda_{k,j(k)}(\mathbf{z})}, \end{aligned} \quad (61)$$

over the trust region (56), (58) and (60), where

$$\begin{aligned} 0 < a_{k,j(k)}^{E,(\kappa)} &= \bar{x}_{k,j(k)}^{E,(\kappa)} b_{k,j(k)}^{E,(\kappa)} - \ln \left( 1 + \bar{x}_{k,j(k)}^{E,(\kappa)} \right), \\ 0 < b_{k,j(k)}^{E,(\kappa)} &= 1 / (1 + \bar{x}_{k,j(k)}^{E,(\kappa)}), \\ \bar{x}_{k,j(k)}^{E,(\kappa)} &= 1 / t_1^{(\kappa)} p_{k,j(k)}^{(\kappa)} \nu_{k,j(k)}^E(\tau^{(\kappa)}, p^{(\kappa)}, p^{E,(\kappa)}, t^{(\kappa)}), \end{aligned}$$

and  $\lambda_{k,j(k)}(\mathbf{z}) \triangleq z_k + z_{j(k)} + z_k^E + \sigma_E / |g_E|^2$ , which is an affine lower bounding approximation of the nonlinear function  $\tau_k \nu_{k,j(k)}^E(\boldsymbol{\tau}, \mathbf{p}, \mathbf{p}^E, \mathbf{t})$ .

### C. Path-following algorithm

By using (50), (51), (52) and (54), (59), the secrecy throughput functions defined by (42), (43) are lower bounded by the following concave functions:

$$\begin{aligned} r_\ell^S(\boldsymbol{\tau}, \mathbf{p}, \mathbf{p}^E, \mathbf{t}) &\geq r_\ell^{S,(\kappa)}(\boldsymbol{\tau}, \mathbf{p}, \mathbf{p}^E, \mathbf{t}, \mathbf{z}) \\ &\triangleq f_\ell^{(\kappa)}(\boldsymbol{\tau}, \mathbf{p}, \mathbf{t}) - f_\ell^{E,(\kappa)}(\boldsymbol{\tau}, \mathbf{p}, \mathbf{p}^E, \mathbf{t}, \mathbf{z}) \\ &\quad + r_{\ell,c}^S, \ell \in \{k, j(k)\}, \end{aligned}$$

under the trust region

$$f_\ell^{(\kappa)}(\boldsymbol{\tau}, \mathbf{p}, \mathbf{t}) - f_\ell^{E,(\kappa)}(\boldsymbol{\tau}, \mathbf{p}, \mathbf{p}^E, \mathbf{t}, \mathbf{z}) \geq 0, \ell \in \{k, j(k)\}. \quad (62)$$

Also, by using (52) and (61), the nonconvex constraint (44) is innerly approximated by the convex constraint

$$\mathbf{r}_{k,c}^S + \mathbf{r}_{j(k),c}^S \leq f_{i,k,j(k)}^{(\kappa)}(\boldsymbol{\tau}, \mathbf{p}) - f_{k,j(k)}^{E,(\kappa)}(\boldsymbol{\tau}, \mathbf{p}, \mathbf{p}^E, \mathbf{t}, \mathbf{z}), i = 1, 2. \quad (63)$$

At the  $\kappa$ -th iteration the following convex optimization problem is solved to generate the next feasible point  $(\tau^{(\kappa+1)}, p^{(\kappa+1)}, p^{E,(\kappa+1)}, t^{(\kappa+1)}, r_c^{S,(\kappa+1)})$  for (49):

$$\begin{aligned} &\max_{\substack{\boldsymbol{\tau} \in \mathbb{R}_+^{K/2}, \mathbf{p} \in \mathbb{R}_+^{3K/2}, \\ \mathbf{p}^E \in \mathbb{R}_+^{K/2}, \mathbf{t} \in \mathbb{R}_+^2, \\ \mathbf{r}_c^S \in \mathbb{R}_+^K, \mathbf{z} \in \mathbb{R}_+^{3K/2}}} f^{S,(\kappa)}(\boldsymbol{\tau}, \mathbf{p}, \mathbf{p}^E, \mathbf{t}, \mathbf{r}_c^S, \mathbf{z}) = \\ &\min_{k=1, \dots, K/2} \min \left\{ r_k^{S,(\kappa)}(\boldsymbol{\tau}, \mathbf{p}, \mathbf{p}^E, \mathbf{t}, \mathbf{z}), \right. \\ &\quad \left. r_{j(k)}^{S,(\kappa)}(\boldsymbol{\tau}, \mathbf{p}, \mathbf{p}^E, \mathbf{t}, \mathbf{z}) \right\} \quad (64a) \\ &\text{s.t.} \quad (45) - (48), (49c), (56) - (58), \\ &\quad (60), (62), (63). \quad (64b) \end{aligned}$$

Algorithm 3, which like Alg. 1 converges at least to a locally optimal solution of the nonconvex problem (49), summarizes the proposed computation. The computational complexity of (64) can be expressed as (25) for  $n = 5K + 2$  and  $m = 4K + 5$ .

---

### Algorithm 3 Information and AN transfer algorithm

---

- 1: **Initialization:** Set  $\kappa = 0$ . Take any feasible point  $(\tau^{(0)}, p^{(0)}, p^{E,(0)}, t^{(0)}, r_c^{S,(0)})$  for the convex constraints (15c), (45)-(48),
  - 2: **Repeat until convergence:** Solve the convex optimization problem (64) to generate the next feasible point  $(\tau^{(\kappa+1)}, p^{(\kappa+1)}, p^{E,(\kappa+1)}, t^{(\kappa+1)}, r_c^{S,(\kappa+1)})$  for (49). Set  $\kappa := \kappa + 1$ .
  - 3: **Output**  $(\tau^{(\kappa)}, p^{(\kappa)}, p^{E,(\kappa)}, t^{(\kappa)}, r_c^{S,(\kappa)})$  as the optimal solution of (49).
- 

## IV. NUMERICAL EXAMPLES

This section presents simulation to show the performance of our proposed methods. There are  $K = 20$  UEs, which are randomly placed within the cell of the radius  $R = 300$  meters. Specifically,  $K/2$  nearer UEs are randomly placed within the circle of the radius 110 meters, while the remaining  $K/2$  UEs are randomly placed in a concentric zone with the radius ranging from 240 to 300 meters. The UAV altitude is  $h = 150$  meters and the antenna beamwidth is set to  $2\pi/5$  rad. The channel power gain at a distance of 1 meter incorporates  $1.42 \times 10^{-4}$  path loss and antenna gain 2.2846 [40]. The Rician factor  $K_R = 10$  is set and the path loss exponent is  $\alpha = 2$  [35]. Other settings are  $\sigma_n^2 = \sigma_e^2 = -174$  dBm/Hz for the noise power density, and  $\epsilon = 10^{-4}$  for the algorithms' convergence.

To weight the pros and cons of each particular signaling scheme, we consider two scenarios for UEs. In the first scenario called UE scenario I, each nearer UE is paired with a farther UE so that the channel conditions of the paired UEs are distinct. In the second scenario called UE scenario II, only  $K/2$  nearer users are considered and served, which are in

similar channel conditions. Thus, in scenario II, any UE is paired with its nearest UE, so that the channel conditions of the paired UEs are similar. HKS-1, NOMA-1, and OMA-1 refer to HKS, NOMA and OMA under the UE scenario I, while HKS-2, NOMA-2, and OMA-II refer to HKS, NOMA and OMA under the UE scenario II.

#### A. Max-min users secrecy throughput optimization over the whole bandwidth

This subsection analyzes the users' achievable minimum normal and secrecy throughput under the EV's overhearing over the whole bandwidth as described Section II. Fig. 2 plots the achievable UEs' minimum secrecy throughput and normal throughput versus the transmit power budget  $P$  under UE scenario I. The achievable UEs' minimum secrecy throughput increases with the transmit power budget  $P$  in all schemes, but of course is worse than the achievable UEs' minimum normal throughput. For both kinds of throughput, the HKS's performance coincides with that of NOMA while the OMA's performance is the worst. Thus, NOMA is preferred as it is simpler than HKS.

Fig. 3 plots the achievable UEs' minimum secrecy throughput and normal throughput versus the transmit power budget  $P$  under UE scenario II. It is clear from Fig. 3 that HKS significantly outperforms NOMA and OMA, while NOMA's performance is almost the same as OMA's. This is quite expected because NOMA is not efficient under similar UEs' channel conditions with this UE scenario. Thus, HKS is preferred in this scenario.

Fig. 4 plots the bandwidth allocations  $\tau_k$  in HKS-1, OMA-1, and NOMA-1 with  $P = 20$  dBm. Note that UE  $k$  and UE  $j(k) = k + K/2$  share the fraction  $\tau_k$  in HKS-1 and NOMA-1, but all UEs are allocated by separate bandwidths under OMA-1. The allocations under HKS-1 and NOMA-1 are seen similar. In addition, Fig. 5 plots the power allocation to the UEs. Under NOMA-1, the information  $s_k$  for the farther UE  $k \in \{1, \dots, K/2\}$  is allocated a very small power  $p_k$  because there is already no interference in decoding it. Fig. 5 also shows that most of power is allocated to the common message  $s_{k,j(k)}$  (the power column for UEs  $k \in \{1, \dots, K/2\}$  is  $p_{k,j(k)}$ , which is allocated to  $s_{k,j(k)}$ ).

Fig. 6 plots the secrecy throughput  $r_k(\boldsymbol{\tau}, \mathbf{p}) - \rho_k^E(\mathbf{p})$  and  $r_{j(k)}(\boldsymbol{\tau}, \mathbf{p}) - \rho_{j(k)}^E(\mathbf{p})$  of the private messages  $s_k$  and  $s_{j(k)}$  in (3), while Fig. 7 plots the split secrecy throughput  $\boldsymbol{\rho}_{k,c}$  in (12) and (13) for  $P = 20$  dBm. By (14),  $\boldsymbol{\rho}_{k,c} + \boldsymbol{\rho}_{j(k),c}$  is the secrecy throughput of the common message  $s_{k,j(k)}$  in (3). One can see that the throughput of the farther UE  $j(k)$  comes from the throughput of the common message  $s_{k,j(k)}$  mainly but not from the throughput of its private message  $s_{j(k)}$ . Meanwhile, Fig. 7 also shows that the throughput of the nearer UE  $k$  is still beneficial from decoding the common message  $s_{k,j(k)}$ . When the channel conditions of UE  $k$  and UE  $j(k)$  are differentiated, such benefit is not sizable because NOMA-1, which allocates the entire throughput of the common message  $s_{k,j(k)}$  to UE  $j(k)$ , achieves similar UEs' secrecy throughput according to Fig. 2. However, the performances of HKS and NOMA will be differentiated if the channel conditions of UE  $k$  and UE  $j(k)$

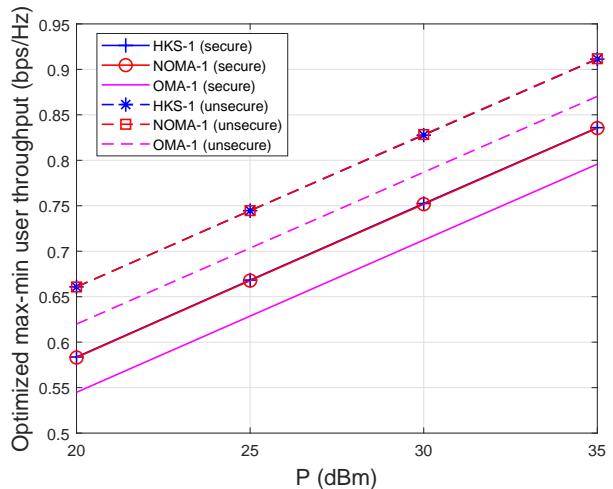


Fig. 2. Achievable UEs' minimum throughput versus the transmitted power budget  $P$  under UE scenario I.

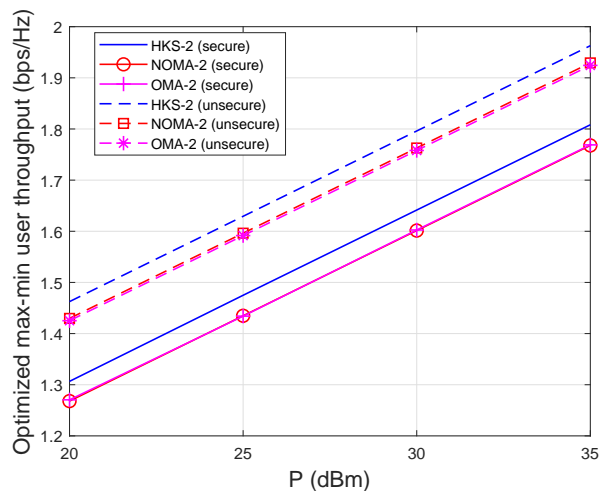


Fig. 3. Achievable UEs' minimum throughput versus the transmitted power budget  $P$  under UE scenario II.

are not differentiated. According to Fig. 3, NOMA-2 cannot perform better than OMA-2 and both of them are clearly outperformed by HKS-2, under which all UEs are beneficial from decoding the common message  $s_{k,j(k)}$  according to Fig. 8.

#### B. Max-min users secrecy throughput optimization over allocated bandwidths

Next, this subsection evaluates the achievable minimum user secrecy throughput under the EV's overhearing over the allocated bandwidths as described in Section III. Fig. 9 plots the trend of the achievable UEs' minimum secrecy throughput and normal throughput versus the transmit power budget  $P$  under UE scenario I. As expected, HKS-1 and NOMA-1 perform similarly and outperform OMA-1 thanks to the UEs' differentiated channel conditions. Besides, we examine the impact of the UAV altitude on the achievable UEs' minimum secrecy throughput and normal throughput. From Fig. 10,

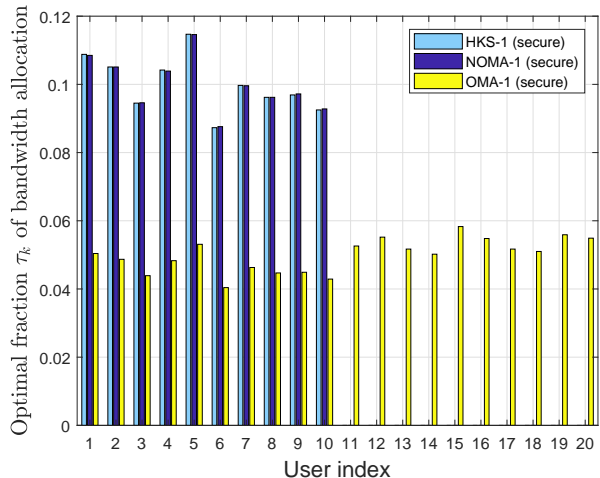


Fig. 4. Optimal fraction  $\tau_k$  of bandwidth allocation under UE scenario I.

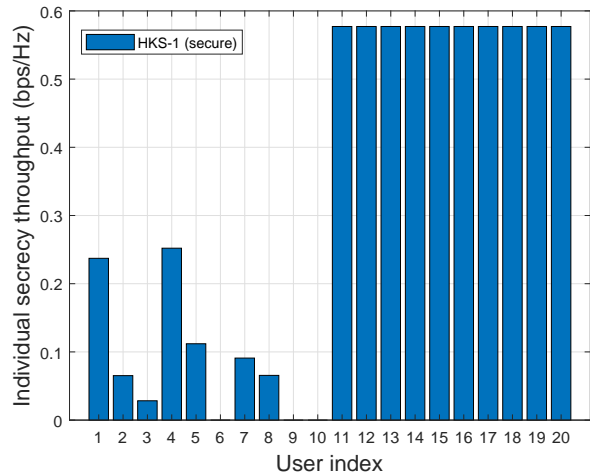


Fig. 7. Individual split secrecy throughput  $\rho_{k,c}$  under HKS-1

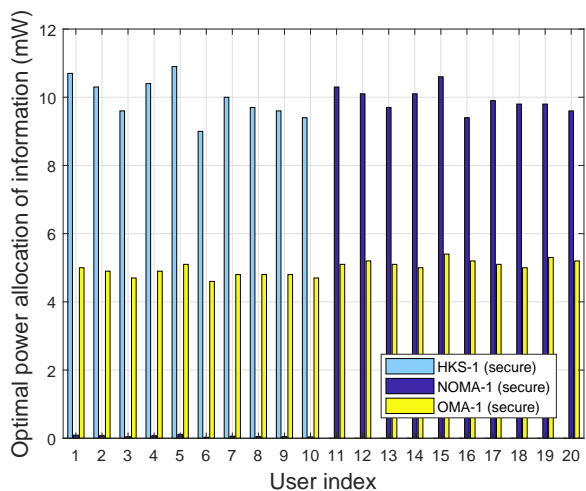


Fig. 5. Optimal power allocation of information transfer under UE scenario I.

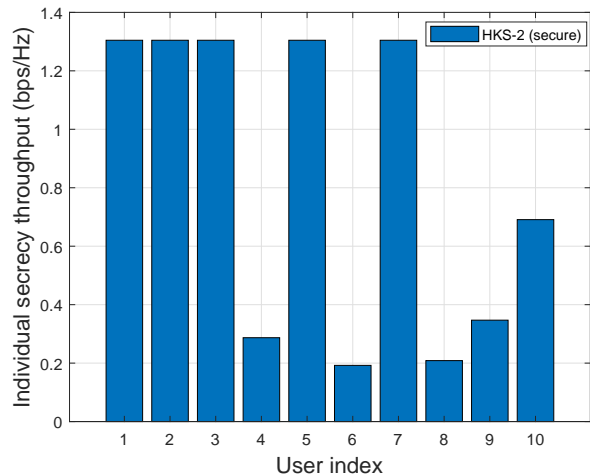


Fig. 8. Individual split secrecy throughput  $\rho_{k,c}$  under HKS-2

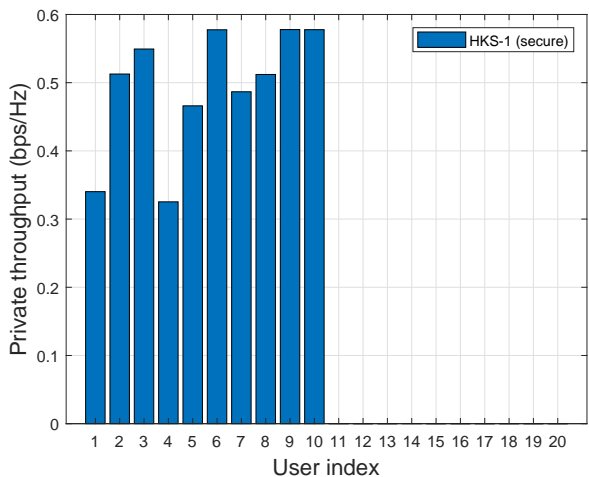


Fig. 6. Private secrecy throughput  $r_k(\boldsymbol{\tau}, \mathbf{p}) - \rho_k^E(\mathbf{p})$  under HKS-1.

it can be seen that the achievable UEs' minimum secrecy throughput and normal throughput decrease with the UAV altitude in all schemes. To the normal throughput, the feasible lowest attitude undoubtedly results in the best performance, since the channel attenuation is the smallest.

Fig. 11 plots these throughput under UE scenario II with similar channel conditions, which shows that HKS-2 clearly outperforms NOMA-2 and OMA-3. The latter two perform similarly.

Fig. 12 plots the bandwidth allocation  $1/\tau_k$  for max-min secrecy throughput optimization in HKS-1, NOMA-1, and OMA-1 with  $P = 20$  dBm. Recall that each UE is allocated a separate bandwidth under OMA-1. Similar bandwidth allocations are observed with HKS-1 and NOMA-1. Further, Fig. 13 plots the power allocation to each UE. Like Fig. 5, NOMA-1 needs to allocate a very small power to the private messages for the nearer UEs, while HKS-1 allocates most power to the common messages. Fig. 14 plots the power allocation to AN transfer to confuse the EV. Compared to Fig. 13, it can be seen that AN is allocated more power than the information

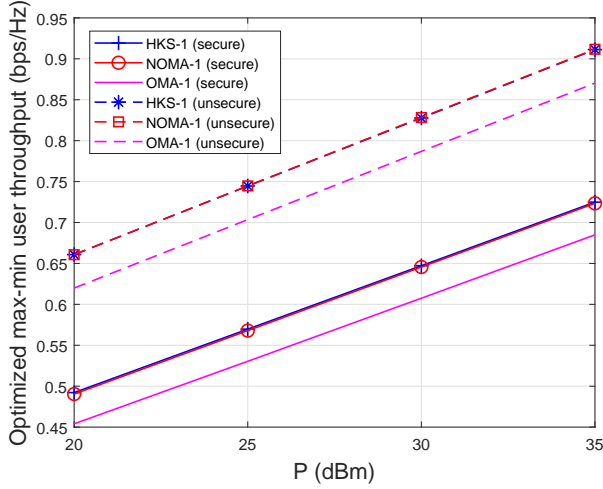


Fig. 9. Achievable UEs' minimum throughput versus the transmitted power budget  $P$  under UE scenario I.

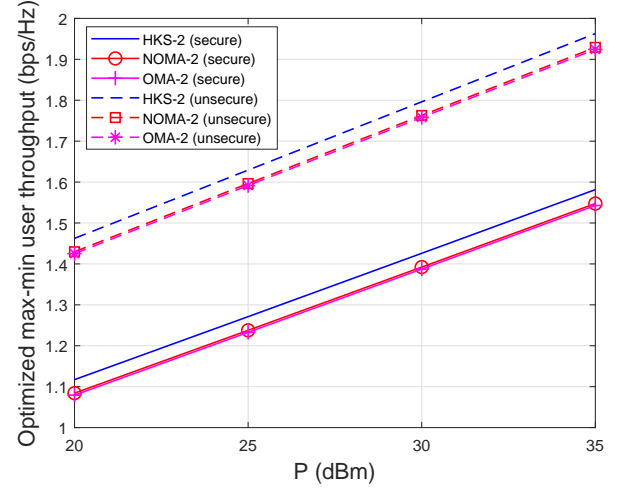


Fig. 11. Achievable UEs' minimum throughput versus the transmitted power budget  $P$  under UE scenario II.

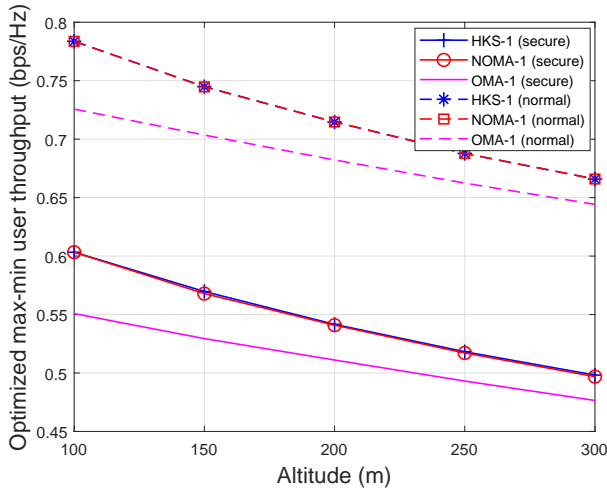


Fig. 10. Achievable UEs' minimum throughput versus the UAV altitude  $h$  under UE scenario I.

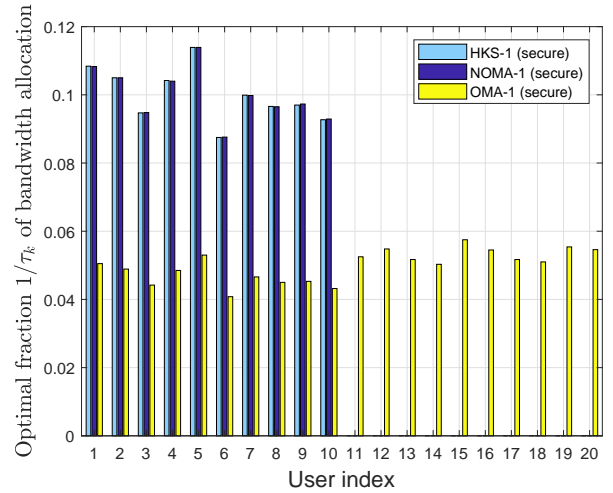


Fig. 12. Optimal fraction  $1/\tau_k$  of bandwidth allocation under UE scenario I.

messages are. HKS-1 and NOMA-1 result in similar power allocation to AN. Fig. 15 plots the total power allocation of each pair under UE scenario I. Under OMA-1, since each UE has distinct bandwidth, each UE communicates with the UAV separately. The total power allocation under HKS-1 is seen similarly to that under NOMA-1.

### C. Algorithm convergence

The convergence behavior of Algorithm 1 is illustrated by Fig. 16. Obviously, the achievable UEs' minimum secrecy throughput converges monotonically after each iteration. It is observed that OMA achieves the fastest convergence rate under each UE scenario, where OMA-1 and OMA-2 require 9 iterations and 13 iterations, respectively. In addition, NOMA-1 and NOMA-2 take no more than 20 iterations to converge. HKS-2 experiences a bit slow iterations to achieve better UEs' minimum secrecy throughput.

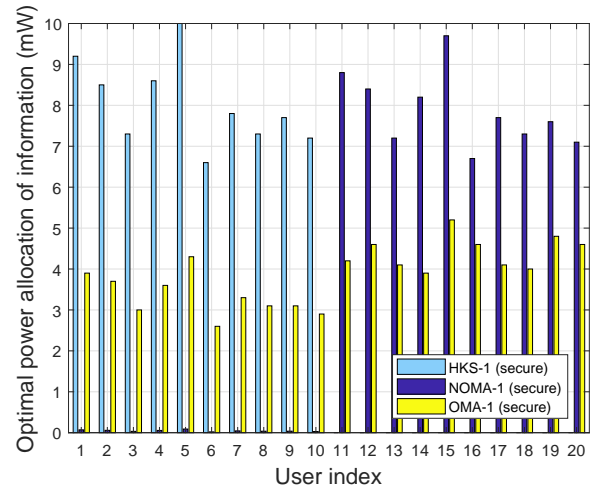


Fig. 13. Optimal power allocation of information transfer under UE scenario I.

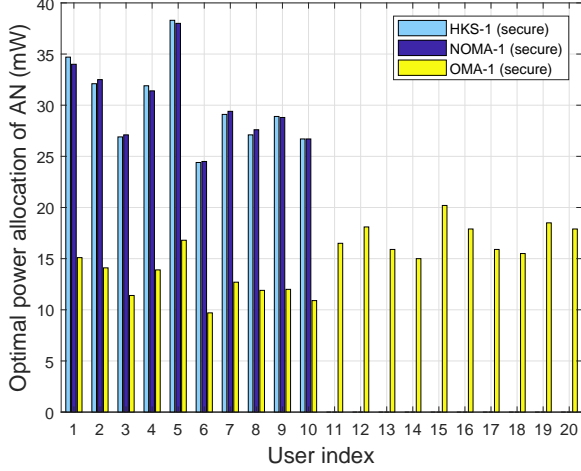


Fig. 14. Optimal power allocation of AN transfer under UE scenario I.

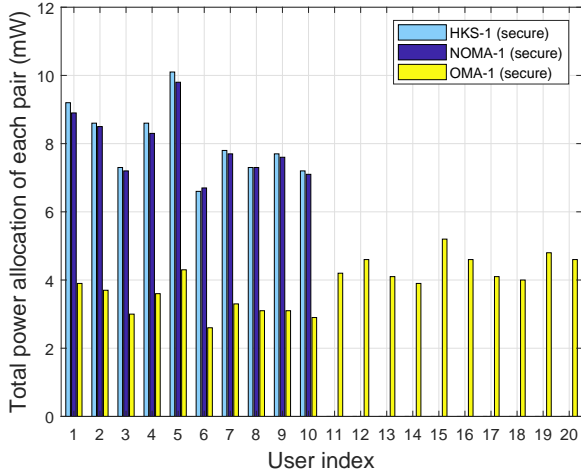


Fig. 15. Total power allocation of each pair under UE scenario I.

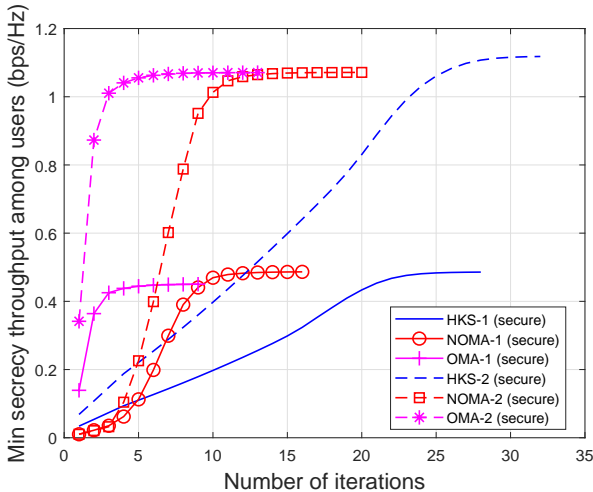


Fig. 16. Convergence of the proposed Algorithms.

## V. CONCLUSIONS

In this paper, we have considered the physical layer security for UAV-enable multi-user communication. The HKS has been first proposed for UAV-enable communication, which can outperform both NOMA and OMA in terms of users throughput. Since it is impossible to insert the AN in the null space of the desired users channel for a single-antenna UAV, a new scheme of information and AN transfer has been proposed to ensure secure communication. The problem of jointly optimizing the time-fraction, power, and bandwidth allocation to maximize the users minimum secrecy throughput has been solved by the efficient path-following algorithms with new inner approximation techniques. Numerical results show the effectiveness of our proposed methods and algorithms. Considering wide-area coverage applications, the problem of UAV trajectory design along with the joint optimization of time-fraction, power, and bandwidth allocation allocation can be the subject of future research.

### APPENDIX: FUNDAMENTAL INEQUALITIES

The following inequalities were proved in [41]

$$\frac{1}{\tau} \ln(1 + 1/xy) \geq \frac{2}{\bar{\tau}} \ln(1 + 1/\bar{x}\bar{y}) + \frac{1}{(1 + \bar{x}\bar{y})\bar{\tau}} (2 - x/\bar{x} - y/\bar{y}) - \frac{\ln(1 + 1/\bar{x}\bar{y})}{\bar{\tau}^2} \tau \quad (65)$$

and

$$\frac{\ln(1 + 1/xy)}{zt} \geq 3 \frac{\ln(1 + 1/\bar{x}\bar{y})}{\bar{z}\bar{t}} + \frac{1}{(\bar{x}\bar{y} + 1)\bar{z}\bar{t}} (2 - \frac{x}{\bar{x}} - \frac{y}{\bar{y}}) - \frac{\ln(1 + 1/\bar{x}\bar{y})}{\bar{z}^2\bar{t}} z - \frac{\ln(1 + 1/\bar{x}\bar{y})}{\bar{z}\bar{t}^2} t. \quad (66)$$

and

$$\ln(1 + x) \leq \ln(1 + \bar{x}) - \frac{\bar{x}}{\bar{x} + 1} + \frac{x}{\bar{x} + 1} \quad (67)$$

for all  $x > 0, y > 0, \tau > 0$  and  $\bar{x} > 0, \bar{y} > 0, \bar{\tau} > 0$ .

Another inequality

$$\frac{1}{xyz} \geq \frac{1}{\bar{x}\bar{y}\bar{z}} \left( 4 - \frac{x}{\bar{x}} - \frac{y}{\bar{y}} - \frac{z}{\bar{z}} \right) \quad \forall x > 0, y > 0, z > 0, \bar{x} > 0, \bar{y} > 0, \bar{z} > 0 \quad (68)$$

follows from the convexity of the function  $1/xyz$  on the domain  $x > 0, y > 0$  and  $z > 0$ .

Replacing  $1/\tau \rightarrow \tau, 1/\bar{\tau} \rightarrow \bar{\tau}$  and  $1/x \rightarrow x$  and  $1/\bar{x} \rightarrow \bar{x}$  in (65) leads to

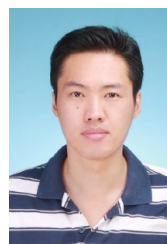
$$\tau \ln(1 + x/y) \geq 2\bar{\tau} \ln(1 + \bar{x}/\bar{y}) + \frac{\bar{\tau}\bar{x}}{\bar{x} + \bar{y}} (2 - \bar{x}/x - y/\bar{y}) - \frac{\ln(1 + \bar{x}/\bar{y})}{\bar{\tau}^2} \tau \quad \forall x > 0, y > 0, \tau > 0, \bar{x} > 0, \bar{y} > 0, \bar{\tau} > 0. \quad (69)$$

Replacing  $x \rightarrow x/y$  and  $\bar{x} \rightarrow \bar{x}/\bar{y}$  leads to

$$\begin{aligned} \ln(1 + x/y) &\leq \ln(1 + \bar{x}/\bar{y}) - \frac{\bar{x}/\bar{y}}{\bar{x}/\bar{y} + 1} + \frac{x}{y(\bar{x}/\bar{y} + 1)} \\ &\leq \ln(1 + \bar{x}/\bar{y}) - \frac{\bar{x}/\bar{y}}{\bar{x}/\bar{y} + 1} + \frac{0.5(x^2/\bar{x} + \bar{x})}{y(\bar{x}/\bar{y} + 1)}. \end{aligned} \quad (70)$$

## REFERENCES

- [1] Y. Saito, Y. Kishiyama, A. Benjebbour, T. Nakamura, A. Li, and K. Higuchi, "Non-orthogonal multiple access (NOMA) for cellular future radio access," in *Proc. IEEE Veh. Technol. Conf. (VTC Spring)*, June 2013, pp. 1–5.
- [2] Z. Ding, F. Adachi, and H. V. Poor, "The application of MIMO to non-orthogonal multiple access," *IEEE Trans. Wirel. Commun.*, vol. 15, no. 1, pp. 537–552, Jan. 2016.
- [3] V.-D. Nguyen, H. D. Tuan, T. Q. Duong, H. V. Poor, and O.-S. Shin, "Precoder design for signal superposition in MIMO-NOMA multicell networks," *IEEE J. Sel. Areas Commun.*, vol. 35, no. 12, pp. 2681–2695, Dec. 2017.
- [4] T. Han and K. Kobayashi, "A new achievable rate region for the interference channel," *IEEE Trans. Inf. Theory*, vol. 27, no. 1, pp. 49–60, Jan. 1981.
- [5] H. Dahrouj and W. Yu, "Coordinated beamforming for the multicell multi-antenna wireless system," *IEEE Trans. Wirel. Commun.*, vol. 9, no. 5, pp. 1748–1759, May 2010.
- [6] E. Che, H. D. Tuan, H. H. M. Tam, and H. H. Nguyen, "Successive interference mitigation in multiuser MIMO interference channels," *IEEE Trans. Commun.*, vol. 63, no. 6, pp. 2185–2199, June 2015.
- [7] H. D. Tuan, H. H. M. Tam, H. H. Nguyen, T. Q. Duong, and H. V. Poor, "Superposition signaling in broadcast interference networks," *IEEE Trans. Commun.*, vol. 65, no. 11, pp. 4646–4656, Nov. 2017.
- [8] H. D. Tuan, A. A. Nasir, M. N. Nguyen, and M. Masood, "Han-Kobayashi signaling in MIMO broadcasting," *IEEE Commun. Lett.*, vol. 23, no. 5, pp. 855–858, 2019.
- [9] H. V. Poor, "Information and inference in the wireless physical layer," *IEEE Commun. Mag.*, vol. 19, no. 2, pp. 40–47, Feb. 2012.
- [10] H. V. Poor and R. F. Schaefer, "Wireless physical layer security," *Proc. Nat. Acad. Sciences USA*, vol. 114, no. 1, pp. 19–26, 2017.
- [11] D. Wang, B. Bai, W. Zhao, and Z. Han, "A survey of optimization approaches for wireless physical layer security," *IEEE Commun. Surveys Tuts.*, vol. 21, no. 2, Secondquarter 2019.
- [12] K. Cumanan, G. C. Alexandropoulos, Z. Ding, and G. K. Karagiannidis, "Secure communications with cooperative jamming: Optimal power allocation and secrecy outage analysis," *IEEE Trans. Veh. Technol.*, vol. 66, no. 8, pp. 7495–7505, Aug 2017.
- [13] A. A. Nasir, H. D. Tuan, T. Q. Duong, and H. V. Poor, "Secrecy rate beamforming for multicell networks with information and energy harvesting," *IEEE Trans. Signal Process.*, vol. 65, no. 3, pp. 677–689, Feb. 2017.
- [14] N. T. Nghia, H. D. Tuan, T. Q. Duong, and H. V. Poor, "MIMO beamforming for secure and energy-efficient wireless communication," *IEEE Signal Process. Lett.*, vol. 24, no. 2, pp. 236–239, Feb. 2017.
- [15] Z. Sheng, H. D. Tuan, T. Q. Duong, and H. V. Poor, "Beamforming optimization for physical layer security in miso wireless networks," *IEEE Trans. Signal Process.*, vol. 66, no. 14, pp. 3710–3723, Jul. 2018.
- [16] L. Gupta, R. Jain, and G. Vaszkun, "Survey of important issues in UAV communication networks," *IEEE Commun. Surveys Tuts.*, vol. 18, no. 2, pp. 1123–1152, Secondquarter 2016.
- [17] M. Mozaffari, W. Saad, M. Bennis, and M. Debbah, "Mobile unmanned aerial vehicles (UAVs) for energy-efficient internet of things communications," *IEEE Trans. Wirel. Commun.*, vol. 16, no. 11, pp. 7574–7589, Nov. 2017.
- [18] X. Lin *et al.*, "The sky is not the limit: LTE for unmanned aerial vehicles," *IEEE Commun. Mag.*, vol. 56, no. 4, pp. 204–210, 2018.
- [19] A. A. Nasir, H. D. Tuan, T. Q. Duong, and H. V. Poor, "UAV-enabled communication using NOMA," *IEEE Trans. Commun.*, vol. 67, no. 7, pp. 5126–5138, Jul. 2019.
- [20] Y. Liu, Z. Qin, Y. Cai, Y. Gao, G. Y. Li, and A. Nallanathan, "UAV communications based on non-orthogonal multiple access," *IEEE Wirel. Commun.*, vol. 26, no. 1, pp. 52–57, 2019.
- [21] H. Liu, S.-J. Yoo, and K. S. Kwak, "Opportunistic relaying for low-altitude UAV swarm secure communications with multiple eavesdroppers," *J. of Commun. and Networks*, vol. 20, no. 5, pp. 496–508, 2018.
- [22] J. Ye, C. Zhang, H. Lei, G. Pan, and Z. Ding, "Secure UAV-to-UAV systems with spatially random UAVs," *IEEE Wirel. Commun. Lett.*, vol. 8, no. 2, pp. 564–567, April 2019.
- [23] M. Cui, G. Zhang, Q. Wu, and D. W. K. Ng, "Robust trajectory and transmit power design for secure UAV communications," *IEEE Trans. Veh. Tech.*, vol. 67, no. 9, pp. 9042–9046, 2018.
- [24] C. Zhong, J. Yao, and J. Xu, "Secure UAV communication with cooperative jamming and trajectory control," *IEEE Commun. Lett.*, vol. 23, no. 2, pp. 286–289, 2019.
- [25] A. Li, Q. Wu, and R. Zhang, "UAV-enabled cooperative jamming for improving secrecy of ground wiretap channel," *IEEE Wirel. Commun. Lett.*, vol. 8, no. 1, pp. 181–184, 2019.
- [26] G. Zhang, Q. Wu, M. Cui, and R. Zhang, "Securing UAV communications via joint trajectory and power control," *IEEE Trans. Wirel. Commun.*, vol. 18, no. 2, pp. 1376–1389, Feb. 2019.
- [27] X. Sun, W. Yang, Y. Cai, Z. Xiang, and X. Tang, "Secure transmissions in millimeter wave SWIPT UAV-based relay networks," *IEEE Wirel. Commun. Lett.*, vol. 8, no. 3, pp. 785–788, Mar. 2019.
- [28] Z. Li, M. Chen, C. Pan, N. Huang, Z. Yang, and A. Nallanathan, "Joint trajectory and communication design for secure UAV networks," *IEEE Commun. Lett.*, vol. 23, no. 4, pp. 636–639, Apr. 2019.
- [29] Y. Cai, F. Cui, Q. Shi, M. Zhao, and G. Y. Li, "Dual-UAV-enabled secure communications: Joint trajectory design and user scheduling," *IEEE J. Sel. Areas Commun.*, vol. 36, no. 9, pp. 1972–1985, 2018.
- [30] H. Lee, S. Eom, J. Park, and I. Lee, "UAV-aided secure communications with cooperative jamming," *IEEE Trans. Veh. Tech.*, vol. 67, no. 10, pp. 9385–9392, 2018.
- [31] X. Zhou, Q. Wu, S. Yan, F. Shu, and J. Li, "UAV-enabled secure communications: Joint trajectory and transmit power optimization," *IEEE Trans. Veh. Technol.*, vol. 68, no. 4, pp. 4069–4073, 2019.
- [32] Y. Cai, Z. Wei, R. Li, D. W. Kwan Ng, and J. Yuan, "Energy-efficient resource allocation for secure UAV communication systems," in *Proc. 2019 IEEE Wireless Communications and Networking Conference (WCNC)*, April 2019, pp. 1–8.
- [33] M. Asadpour, B. van den Bergh, D. Giustiniano, K. Hummel, S. Pollin, and B. Plattner, "Micro aerial vehicle networks: An experimental analysis of challenges and opportunities," *IEEE Commun. Mag.*, vol. 52, no. 7, pp. 141–149, 2014.
- [34] A. A. Nasir, H. D. Tuan, and T. Q. Duong, "Fractional-time exploitation for serving IoT users with guaranteed QoS by 5G spectrum," *IEEE Commun. Mag.*, vol. 56, no. 10, pp. 128–133, Oct. 2018.
- [35] F. Ono, H. Ochiai, and R. Miura, "A wireless relay network based on unmanned aircraft system with rate optimization," *IEEE Trans. Wirel. Commun.*, vol. 15, no. 11, pp. 7699–7708, Nov. 2016.
- [36] W. Huang, Z. Yang, C. Pan, L. Pei, M. Chen, M. Shikh-Bahaei, M. Elkashlan, and A. Nallanathan, "Joint power, altitude, location and bandwidth optimization for UAV with underlaid D2D communications," *IEEE Wirel. Commun. Lett.*, vol. 8, no. 2, pp. 524–527, April 2019.
- [37] H. Tuy, *Convex Analysis and Global Optimization (second edition)*. Springer, 2016.
- [38] B. R. Marks and G. P. Wright, "A general inner approximation algorithm for nonconvex mathematical programs," *Operations Research*, vol. 26, no. 4, pp. 681–683, Jul 1978.
- [39] W. Li, M. Ghogho, B. Chen, and C. Xiong, "Secure communication via sending artificial noise by the receiver: Outage secrecy capacity/region analysis," *IEEE Commun. Lett.*, vol. 16, no. 10, pp. 1628–1631, Oct. 2012.
- [40] H. He, S. Zhang, Y. Zeng, and R. Zhang, "Joint altitude and beamwidth optimization for UAV-enabled multiuser communications," *IEEE Commun. Lett.*, vol. 22, no. 2, pp. 344–347, 2018.
- [41] Z. Sheng, H. D. Tuan, A. A. Nasir, T. Q. Duong, and H. V. Poor, "Power allocation for energy efficiency and secrecy of wireless interference networks," *IEEE Trans. Wirel. Commun.*, vol. 17, no. 6, pp. 3737–3751, Jun. 2018.



**Zhichao Sheng** received the Ph.D. degree in electrical engineering from the University of Technology, Sydney, NSW, Australia in 2018. From 2018 to 2019, he was a Research Fellow at School of Electronics, Electrical Engineering and Computer Science, Queen's University Belfast, Belfast, U.K. He is currently a Lecturer with Shanghai University, Shanghai, China. His research interests include optimization methods for wireless communication and signal processing.



**Hoang Duong Tuan** received the Diploma (Hons.) and Ph.D. degrees in applied mathematics from Odessa State University, Ukraine, in 1987 and 1991, respectively. He spent nine academic years in Japan as an Assistant Professor in the Department of Electronic-Mechanical Engineering, Nagoya University, from 1994 to 1999, and then as an Associate Professor in the Department of Electrical and Computer Engineering, Toyota Technological Institute, Nagoya, from 1999 to 2003. He was a Professor with the School of Electrical Engineering and Telecommunications, University of New South Wales, from 2003 to 2011. He is currently a Professor with the School of Electrical and Data Engineering, University of Technology Sydney. He has been involved in research with the areas of optimization, control, signal processing, wireless communication, and biomedical engineering for more than 20 years.



**H. Vincent Poor** (S'72, M'77, SM'82, F'87) received the Ph.D. degree in EECS from Princeton University in 1977. From 1977 until 1990, he was on the faculty of the University of Illinois at Urbana-Champaign. Since 1990 he has been on the faculty at Princeton, where he is currently the Michael Henry Strater University Professor of Electrical Engineering. During 2006 to 2016, he served as Dean of Princeton's School of Engineering and Applied Science. He has also held visiting appointments at several other universities, including most recently at Berkeley and Cambridge. His research interests are in the areas of information theory, signal processing and machine learning, and their applications in wireless networks, energy systems and related fields. Among his publications in these areas is the recent book *Multiple Access Techniques for 5G Wireless Networks and Beyond*. (Springer, 2019).

Dr. Poor is a member of the National Academy of Engineering and the National Academy of Sciences, and is a foreign member of the Chinese Academy of Sciences, the Royal Society, and other national and international academies. Recent recognition of his work includes the 2017 IEEE Alexander Graham Bell Medal and a D.Eng. *honoris causa* from the University of Waterloo awarded in 2019.



**Ali Arshad Nasir** (S'09-M'13) is an Assistant Professor in the Department of Electrical Engineering, King Fahd University of Petroleum and Minerals (KFUPM), Dhahran, KSA. Previously, he held the position of Assistant Professor in the School of Electrical Engineering and Computer Science (SECS) at National University of Sciences & Technology (NUST), Pakistan, from 2015-2016. He received his Ph.D. in telecommunications engineering from the Australian National University (ANU), Australia in 2013 and worked there as a Research Fellow from 2012-2015. His research interests are in the area of signal processing in wireless communication systems. He is an Associate Editor for IEEE Canadian Journal of Electrical and Computer Engineering.



**Trung Q. Duong** (S'05, M'12, SM'13) received his Ph.D. degree in Telecommunications Systems from Blekinge Institute of Technology (BTH), Sweden in 2012. Currently, he is with Queen's University Belfast (UK), where he was a Lecturer (Assistant Professor) from 2013 to 2017 and a Reader (Associate Professor) from 2018. His current research interests include wireless communications, machine learning, realtime optimisation, big data, and IoT applications to disaster management, air-quality monitoring, flood monitoring, smart agriculture, healthcare and smart cities. He is the author or co-author of over 350+ technical papers published in scientific journals (210+ articles) and presented at international conferences (140+ papers).

Dr. Duong currently serves as an Editor for the IEEE TRANSACTIONS ON WIRELESS COMMUNICATIONS, IEEE TRANSACTIONS ON COMMUNICATIONS, and a Lead Senior Editor for IEEE COMMUNICATIONS LETTERS. He was awarded the Best Paper Award at the IEEE Vehicular Technology Conference (VTC-Spring) in 2013, IEEE International Conference on Communications (ICC) 2014, IEEE Global Communications Conference (GLOBECOM) 2016 and 2019, IEEE Digital Signal Processing Conference (DSP) 2017, and International Wireless Communications & Mobile Computing Conference (IWCMC) 2019. He is the recipient of prestigious Royal Academy of Engineering Research Fellowship (2016-2021) and has won a prestigious Newton Prize 2017.